3

Passive microrheology

3.1 The Langevin equation 86
3.2 Brownian motion 90
3.3 The Generalized Einstein Relation 98
3.4 The Stokes component 103
3.5 The Generalized Stokes–Einstein Relation (GSER) 105
3.6 Passive microrheology examples 107
3.7 GSER for model materials 110
3.8 Converting between the time and frequency domains 118
3.9 Strengths and limitations of passive microrheology 123
3.10 Validity of the GSER 124
3.11 General limits of operation 129
Exercises 132

Passive microrheology is distinct from other micro- and macrorheological measurements, in that it relies on the inherent thermal motion of probe particles that are dispersed within the viscoelastic material of interest. Random thermal forces displace the particles, and the statistics of their subsequent motion encode the surrounding material rheology. We will see in later chapters that this thermal motion can be measured by a number of experimental techniques, including microscopy and light scattering. For now, we will focus on the theoretical basis of passive microrheology because this analysis leads to insight into its strengths and a few important limitations.

The Generalized Stokes–Einstein Relation (GSER) is the principal defining equation of passive microrheology. It is a physical relation between the thermal motion of probe particles and the material rheology. Specifically, it relates the observable *displacement* of the probe particles to the surrounding material's rheological response.

The derivation of the GSER consists of two important components: First is the Einstein relation, which states that the thermally fluctuating motion of probe particles is related to the resistance imposed on the probe by the surrounding material. The second component is the generalized Stokes drag (Chapter 2), which is used to calculate the stresses exerted by the material on the probe. Both the Einstein relation and the Stokes equation make assumptions regarding the material that warrant explicit discussion, since these impose limitations on the samples that can be measured using passive microrheology.

We begin this chapter by discussing the Langevin equation, the equation of motion from which the GSER is derived. After deriving the Stokes–Einstein relation and the GSER, we discuss the interpretation of passive microrheology experiments and its operating regime.

3.1 The Langevin equation

A discussion of the Langevin equation precedes our detailed development of the Stokes–Einstein relationship in Section 3.2. Our primary interest is to develop the equation of motion for probe particles and

Microrheology. Eric M. Furst and Todd M. Squires, Oxford University Press (2017).
 DOI 10.1093/oso/9780199655205.001.0001

understanding the contributions of the random thermal force and the dissipative forces.

Consider a tracer particle suspended in a viscoelastic medium. When a force **f** is exerted on the particle, we expect it to move, subject to the resistance of the surrounding material. The equation of motion—Newton's second law—is[1]

$$M_p \dot{\mathbf{V}}(t) = \mathbf{f} - \int_{-\infty}^{t} \zeta(t-t')\mathbf{V}(t')dt', \tag{3.1}$$

where $M_p = (4\pi/3)a^3\rho_p$ is the particle mass.

The second term in eqn 3.1 reflects the resistance exerted on the particle by the surrounding material, written as a convolution of the instantaneous velocity $\mathbf{V}(t)$ with the microscopic resistance $\zeta(t)$. We will derive this function in Section 3.5 when we discuss the Stokes component in detail. The resistance function accounts for both the viscous and elastic stresses exerted on the probe. Obviously, a particle suspended in a viscous medium will stop moving in the absence of an applied force **f**; the velocity must decay eventually to zero.

Before we proceed, note the limits of the resistance function integral in eqn 3.1. Specifying the lower limit of integration as $t = -\infty$, effectively states that the particle is in thermodynamic equilibrium at $t = 0$. Consequently, the resistance function must obey

$$\zeta(t) = 0, \ t < 0. \tag{3.2}$$

to ensure that causality is not violated. The particle cannot be subjected to resistance forces generated by future velocities!

For now, consider the resistance function for a purely viscous fluid, accelerating slowly enough that inertial forces may be neglected. The resistance is solely due to the viscous drag force, which depends only on the instantaneous velocity. The memory function in this case is

$$\zeta(t) = \zeta_0 \delta(t), \tag{3.3}$$

where ζ_0 is a constant and $\delta(t)$ is the Dirac delta function, and eqn 3.1 becomes

$$M_p \dot{\mathbf{V}}(t) = \mathbf{f} - \zeta_0 \mathbf{V}(t). \tag{3.4}$$

In Section 2.5.2, the Stokes drag on a sphere translating in a Newtonian liquid of viscosity η was shown to be $\zeta = 6\pi a\eta$ for no-slip (solid) spheres, and $\zeta = 4\pi a\eta$ for perfectly slipping spheres (*e.g.*, bubbles). Note, however, that the quasi-steady Stokes drag eqn 3.4 is only valid

[1] Kubo *et al.* (1991) and Zwanzig and Bixon (1970) are excellent references for their detailed treatments of the Langevin equation and Brownian motion.

on time scales greater than the viscous-relaxation time scale $\rho_f a^2/\eta$, where ρ_f is the fluid density, as shown in section 2.5.3.

Under a constant imposed force such that the particle is not accelerating, the simplified equation of motion can be solved for the velocity by a straightforward rearrangement,[2]

$$\mathbf{V}(t) = \mathbf{f}/\zeta_0. \tag{3.5}$$

In fact, under most circumstances, the particle inertia is so small that the first term in eqn 3.1 is negligible. Only on very short time scales ($t \sim M_p/\zeta_0$ in the viscous fluid) do we need to consider particle (and fluid) inertia. We can demonstrate this by considering a time-dependent force $\mathbf{f}(t)$. Equation 3.1 can be solved formally to give the velocity

$$\mathbf{V}(t) = \mathbf{V}(0)e^{-\zeta_0 t/M_p} + \frac{1}{M_p}\int_0^t e^{-\frac{\zeta_0}{M_p}(t-t')}\mathbf{f}(t')dt'. \tag{3.6}$$

An impulsive force,

$$\mathbf{f}(t) = \frac{M_p}{\zeta_0}\mathbf{f}_0\delta(t), \tag{3.7}$$

exerted on a particle initially at rest, $\mathbf{v}(0) = \mathbf{0}$, drives the particle with velocity

$$\mathbf{V}(t) = (\mathbf{f}_0/\zeta)e^{-\zeta_0 t/M_p}. \tag{3.8}$$

The particle moves initially with velocity f_0/ζ_0, which then decreases exponentially until the particle comes to rest, over a relaxation time scale $\tau = M_p/\zeta_0$. For a one micrometer diameter particle dispersed in water, the relaxation time scale is quite small, $M_p/\zeta_0 \sim 10^{-8}$ s—on the order of only a hundredth of a microsecond!

The **Langevin equation** is no more than eqn 3.4 with one peculiarity—that the force is a random, fluctuating force $\mathbf{f}_B$ that results from the thermal motion of the surrounding molecules. In a similar way, inserting a random force $\mathbf{f}_B$ in eqn 3.1, which does not assume a form for $\zeta(t)$, gives rise to the **Generalized**-Langevin equation.The random force is assumed to have random direction and magnitude (over sufficiently long time scales), so that its time average is zero,

$$\langle \mathbf{f}_B(t) \rangle = \mathbf{0}. \tag{3.9}$$

[2] See Exercise 1 for the response in an elastic solid.

For purely viscous fluids that obey eqn 3.4, the random force is also assumed to be *uncorrelated*[3] with velocity,

$$\langle \mathbf{f}_B(t) \cdot \mathbf{V}(t') \rangle = 0. \tag{3.10}$$

The form and time-dependence of the random force $\mathbf{f}_B(t)$ are determined by the details of the collisions of the particle with the surrounding fluid. For viscous fluids obeying eqn 3.4, the random force is only correlated over molecular collision time scales—generally much shorter than time scales for particle motions—and is therefore generally approximated by a delta function,

$$\langle \mathbf{f}_B(t) \cdot \mathbf{f}_B(t') \rangle = F_0 \delta(t - t'), \tag{3.11}$$

where the constant F_0 is proportional to the mean-squared magnitude of the Brownian force. Thermal forces within complex fluids that obey eqn 3.1 exhibit a more complicated time correlation, as discussed by (Kubo *et al.*, 1991) and in Section 3.3.

In this simplest case, the Fourier Transform[4] of eqn 3.11,

$$\langle \tilde{\mathbf{f}}_B(\omega) \cdot \mathbf{f}_B(t') \rangle = \int_{-\infty}^{\infty} e^{-i\omega t} \langle \mathbf{f}_B(t) \cdot \mathbf{f}_B(t') \rangle dt = F_0 e^{-i\omega t'}, \tag{3.12}$$

so that Fourier transforming over t' gives

$$\langle \tilde{\mathbf{f}}_B(\omega) \cdot \tilde{\mathbf{f}}_B(\omega') \rangle = 2\pi F_0 \delta(\omega + \omega'), \tag{3.13}$$

or,

$$\langle \tilde{\mathbf{f}}_B(\omega) \cdot \tilde{\mathbf{f}}_B(-\omega') \rangle = \langle \tilde{\mathbf{f}}_B(\omega) \cdot [\tilde{\mathbf{f}}_B(\omega')]^* \rangle = 2\pi F_0 \delta(\omega - \omega'). \tag{3.14}$$

The power spectral density expresses how much of the distribution is contained within $d\omega$ of a given frequency ω,

$$S_f(\omega) = \langle |\tilde{\mathbf{f}}_B(\omega)|^2 \rangle = \int_{\omega - d\omega/2}^{\omega + d\omega/2} \langle \tilde{\mathbf{f}}_B(\omega) \cdot [\tilde{\mathbf{f}}_B(\omega')]^* \rangle d\omega' \tag{3.15}$$

which in this case is independent of frequency

$$\langle |\tilde{\mathbf{f}}_B(\omega)|^2 \rangle = 2\pi F_0, \tag{3.16}$$

a characteristic of *white noise*. The magnitude of the Brownian force is determined by the requirements of thermal equilibrium, and will now be discussed in Section 3.2.

[3] See Chapter 5 for a discussion of time–correlation functions.

[4] The Fourier Transform is discussed in Appendix A.1.

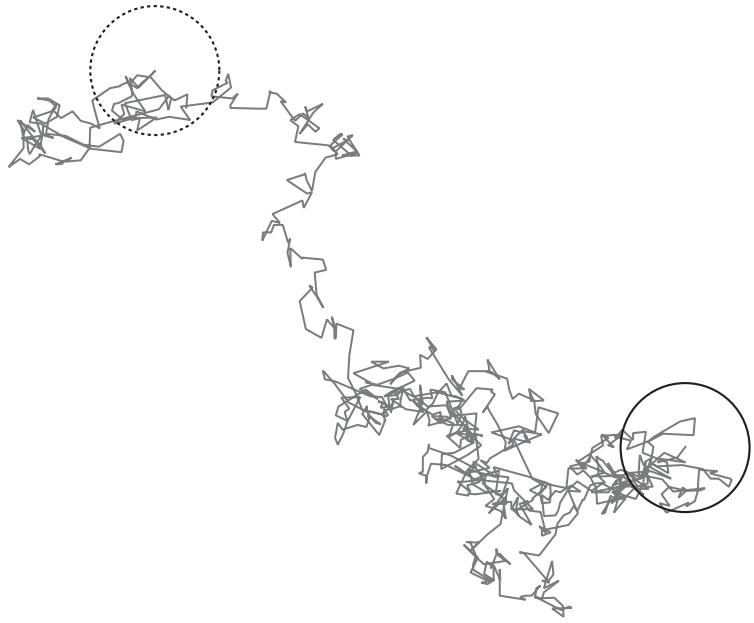

Fig. 3.1 *The trajectory of a Brownian particle is a discontinuous, random walk. The dashed circle is the particle's starting point and the solid circle is its end point.*

Because the Langevin equation is driven by a random, fluctuating force $\mathbf{f}_B$—owing to the stochastic, thermal motion of the surrounding molecules—solutions to the Langevin equation are non-deterministic. Particles that obey the Langevin equation exhibit random walks, an example of which is shown in Fig. 3.1.

As a *stochastic* equation, solutions to the Langevin equation will have the form of statistical (ensemble) averages over many realizations of probe particle trajectories. Before we discuss the general solution of the (generalized) Langevin equation for a viscoelastic material, let us first consider the Brownian motion of particles in a viscous Newtonian fluid.

3.2 Brownian motion

The thermal, or Brownian, force is well known through the perpetual random motion of small particles and, historically, provided direct evidence of the molecular motion inherent in the microscopic understanding of the nature of matter (Maiocchi, 1990; Bigg, 2008).[5] As Einstein demonstrated, the thermal force is also related to the frictional drag force, which arises due to molecules impacting the moving particle (Einstein, 1905). These molecular collisions produce both tangential (shear) forces and normal forces that slow the motion of

[5] Named for the botanist and talented microscopist Robert Brown (1773–1858), who famously described the perpetual random motion of pollen organelles (amyloplasts and spherosomes) and finely ground inorganic particles suspended in water. Brown made his observations in 1827. His account was published in 1829, nearly a century before Einstein published his molecular theory (Brown, 1828).

the particle, which gives rise to the resistance ζ_0 used in the previous section. The relationship between the random thermal force and frictional drag force is a manifestation of the *fluctuation-dissipation theorem* (Kubo, 1966; Kubo *et al.*, 1991).

Solutions to the Langevin equation are not deterministic, because the force $\mathbf{f}_B$ acting on the particle is random and fluctuating. Two approaches are commonly used to solve the Langevin equation, each with distinct advantages and disadvantages. We will explicitly discuss each for the simplest system introduced in the Langevin equation (3.4) for quasi-steady Stokes flow, tracking motion in only one direction (*e.g.*, the x-direction) for simplicity:

$$M_p \dot{V}(t) = f_B - \zeta_0 V. \tag{3.17}$$

We warn, however, that this approach omits the inertia of the fluid, and therefore makes incorrect predictions for any material whose density is not substantially smaller than that of the probe. Nonetheless, this simpler system is clearer pedagogically, and illustrates the conceptual and logical strategies employed to solve the Langevin equation, without many of the mathematical difficulties or subtleties that arise for more general (non-Newtonian, or inertial) materials. Once we have this basic framework in place, we will then describe the proper generalization for more general systems—both non-Newtonian and inertial.

3.2.1 Laplace Transform solutions

We begin by taking the *Laplace* Transform of the Langevin equation (3.4) for quasi-steady Stokes flow, giving

$$sM_p \hat{V}(s) - M_p V(0) = \hat{f}_B(s) - \zeta_0 \hat{V}(s). \tag{3.18}$$

Solving for $\hat{V}(s)$ gives

$$\hat{V}(s) = \frac{\hat{f}_B(s) + M_p V(0)}{\zeta_0 + sM_p}. \tag{3.19}$$

The Laplace Transform naturally introduces the initial velocity $V(0)$, which makes the equipartition theorem relatively easy to invoke. Multiplying eqn 3.19 by the initial velocity $V(0)$, then taking the ensemble average, gives

$$\langle \hat{V}(s) V(0) \rangle = \frac{\langle \hat{f}_B(s) V(0) \rangle + M_p \langle V(0) V(0) \rangle}{\zeta_0 + sM_p}. \tag{3.20}$$

Because the Brownian force has zero average (eqn 3.9) and is assumed to be uncorrelated with particle velocity (eqn 3.10), the first term vanishes, leaving

$$\langle \hat{V}(s) V(0) \rangle = \frac{M_p \langle V(0) V(0) \rangle}{\zeta_0 + s M_p}. \tag{3.21}$$

The equipartition theorem governs the kinetic energy of particles in thermal equilibrium with their surroundings, stating that each independent degree of freedom has energy $\frac{1}{2} k_B T$. Since we are tracking only one-dimensional displacement in this particular example, this yields

$$\frac{1}{2} M_p \langle V(0) V(0) \rangle = \frac{1}{2} k_B T, \tag{3.22}$$

so that

$$\langle \hat{V}(s) V(0) \rangle = \frac{k_B T}{\zeta_0 + s M_p}. \tag{3.23}$$

Taking the inverse transform gives the velocity autocorrelation function (VAC),

$$\langle V(t) V(0) \rangle = \frac{k_B T}{M_p} e^{-\zeta_0 |t| / M_p}. \tag{3.24}$$

Although the mean velocity must be zero for a particle experiencing a random fluctuating force, $\langle V \rangle = 0$, eqn 3.24 shows that the corresponding velocity fluctuations decay on the time scale M_p/ζ_0 identified previously, for the particle's deterministic response to an impulsive force.

Strictly speaking, eqn 3.24 only holds for probes whose density signifiantly exceeds that of the fluid. Much more common in microrheology is when probe and medium densities are of the same order, in which case fluid inertia decays on the same time scale as the particle inertia ($\sim a^2/\nu$, where $\nu = \eta/\rho_f$ is the kinematic viscosity). In that case, the assumption of a constant ζ_0 is therefore flawed, and will be treated properly in Section 3.4.

3.2.2 Fourier Transform solutions

An alternative solution strategy (Kubo *et al.*, 1991; Indei *et al.*, 2012*b*) is to decompose $V(t)$ via a Fourier Transform,

$$V(t) = \frac{1}{2\pi} \int_{-\infty}^{\infty} \tilde{V}(\omega) e^{i\omega t} d\omega, \tag{3.25}$$

which gives

$$i\omega M_p \tilde{V}(\omega) = \tilde{f}_B - \zeta_0 \tilde{V}, \tag{3.26}$$

and therefore

$$\tilde{V}(\omega) = \frac{\tilde{f}_B(\omega)}{\zeta_0 + i\omega M_p}. \tag{3.27}$$

An advantage (but also disadvantage) to the Fourier Transform approach is that it does not single out any time $t = 0$, even if that time is ultimately arbitrary.[6]

To find the velocity autocorrelation function, we compute the ensemble average

$$\langle \tilde{V}(\omega)\tilde{V}^*(\omega')\rangle = \frac{\langle \tilde{f}_B(\omega)\tilde{f}_B^*(\omega')\rangle}{(\zeta_0 + i\omega M_p)(\zeta_0 - i\omega' M_p)}. \tag{3.29}$$

Using eqn 3.14 for the statistics of thermal force exerted on a probe within a quasi-steady, Newtonian liquid gives

$$\langle \tilde{V}(\omega)\tilde{V}^*(\omega')\rangle = 2\pi F_0 \frac{\delta(\omega - \omega')}{(\zeta_0 + i\omega M_p)(\zeta_0 - i\omega' M_p)}. \tag{3.30}$$

Inverse Fourier transforming over ω, using a time $t + \tau$, gives

$$\langle V(t+\tau)\tilde{V}^*(\omega')\rangle = F_0 \frac{e^{i\omega'(t+\tau)}}{\zeta_0^2 + \omega'^2 M_p^2}. \tag{3.31}$$

Taking the complex conjugate and inverse transforming over ω' gives

$$\langle V(t+\tau)V(t)\rangle = \frac{F_0}{2\pi}\int_{-\infty}^{\infty} \frac{e^{-i\omega'\tau}}{\zeta_0^2 + \omega'^2 M_p^2} d\omega', \tag{3.32}$$

which can be integrated (*e.g.*, using residue calculus) to yield

$$\langle V(t+\tau)V(t)\rangle = \frac{F_0}{M_p \zeta_0} e^{-\zeta_0 |\tau|/M_p}. \tag{3.33}$$

Notably, the velocity autocorrelation function depends only on the lag time τ, not on t; which follows from the fact that the thermal force was assumed to be stationary.

The final step is to invoke known properties of thermal equilibrium in order to determine the magnitude of F_0. Computing the VAC at

[6] There is nothing unique about the initial velocity $V(0)$ in this derivation. Because the equilibrium ensemble average is stationary, and the classical-mechanical equations of motion are time reversible, the correlations between dynamical variables like the velocity should depend only on the separation between times, and not the absolute value of time (McQuarrie, 2000; Chandler, 1987). Therefore, we may write

$$\begin{aligned}\langle V(t')V(t'')\rangle &= \langle V(t'-t'')V(0)\rangle \\ &= \langle V(t''-t')V(0)\rangle.\end{aligned} \tag{3.28}$$

zero time lag allows the equipartition theorem eqn 3.22 to be invoked, so that

$$\langle V(t)V(t)\rangle = \frac{k_BT}{M_p} = \frac{F_0}{M_p\zeta_0}, \tag{3.34}$$

meaning

$$F_0 = k_BT\zeta_0, \tag{3.35}$$

so that

$$\langle V(t+\tau)V(t)\rangle = \frac{k_BT}{M_p}e^{-\zeta_0|\tau|/M_p}, \tag{3.36}$$

in agreement with eqn 3.24, found using Laplace Transforms.

Note that eqn 3.35 reveals that the random, fluctuating force exerted on a particle by the collective action of individual, thermally agitated molecules actually "knows" about the determinstic resistance on that particle being forced to move through its environment. Why and how would that information be transmitted to individual molecules, each crashing into its neighbors (and the probe)? The connection is subtle and profound—and reflects the consequences of the fluctuation-dissipation theorem. In short, the forces exerted on the particle by the surrounding molecules perform work on the particle as they do so. In order for the probe to remain in thermal equilibrium with its surroundings, that energy must be dissipated back into the medium, to maintain a net energy balance. The latter (dissipative) step involves the (deterministic) drag resistance ζ that dissipates the energy; and the former introduces k_BT. This topic is explored in Exercise 3.3.

It should come as no surprise that these two methods of solving the Langevin equation give the same answer. It is worth noting, however, how the two approaches differ. By its very nature, the Laplace Transform only incorporates positive times $t > 0$, and therefore the initial condition $V(0)$ enters the Laplace-Transformed Langevin equation 3.18 explicitly. Computing the dot product with $V(0)$, and ensemble averaging, naturally caused the Brownian force term to vanish from the equation, and left the (ensemble-averaged) initial kinetic energy alone in the equation. One need not compute or even consider the magnitude of the Brownian forces explicitly in this approach, since the ensemble-averaged kinetic energy appears directly, and can immediately be related to k_BT via the equipartition theorem.

By contrast, the Fourier-Transform approach incorporates *all* times $-\infty < t < \infty$ in its analysis, and therefore no "initial condition" $V(0)$ is singled out, or ever appears, in its solution. Instead, one computes $\langle\tilde{V}(\omega)\tilde{V}^*(\omega')\rangle$ directly, then inverting both Fourier Transforms.

In so doing, the autocorrelation of the (Fourier-Transformed) Brownian forces $\langle \tilde{\mathbf{f}}_B(\omega)\tilde{\mathbf{f}}_B^*(\omega')\rangle$ is introduced. The statistics of $\mathbf{f}_B(t)$ must therefore be employed directly in the Fourier Transform solution.

The *unilateral*, or *one-sided*, Fourier Transform,

$$\mathscr{F}_u[V(t)] = \int_0^\infty e^{-i\omega t} V(t)\,dt, \tag{3.37}$$

is sometimes used to solve these problems. Like the Laplace Transform, the unilateral Fourier Transform singles out a particular time $t = 0$ as an "initial condition," and only incorporates times $t > 0$ in its analysis. The unilateral Fourier Transform and Laplace Transform can be related via *analytic continuation*, using techniques from Complex Analysis, so long as the transformed functions meet criteria common for microrheology conditions. In particular, the probe response must be causal, meaning that a probe can not respond to a force that has not yet occurred. In practice, analytic continuation involves replacing s in the Laplace Transform with $i\omega$ for the unilateral Fourier Transform

$$\hat{V}(s \to i\omega) = \tilde{V}(\omega) \tag{3.38}$$

$$\tilde{V}(\omega \to -is) = \hat{V}(s). \tag{3.39}$$

See Appendix A.2 for a discussion.

3.2.3 Relating VAC to MSD

We have related the *statistical* properties of probe velocities to the (deterministic) probe resistance ζ_0 for a probe moving in a quasi-steady viscous fluid. In practice, however, it is difficult to measure velocity autocorrelations. A little additional analysis, however, relates the velocity autocorrelation function to quantities that are more amenable to measurement.

For example, particles effectively move via random walks over long time scales, with a diffusivity that can be determined from the velocity autocorrelation function via

$$D_0 = \int_0^\infty \langle V(t)V(0)\rangle dt = \lim_{s\to 0} \mathscr{L}\{\langle V(t)V(0)\rangle\} \tag{3.40}$$

$$= \lim_{s\to 0} \frac{k_B T}{\zeta_0 + M_p s}, \tag{3.41}$$

so that

$$D_0 = \frac{k_B T}{\zeta_0} \equiv \frac{k_B T}{6\pi\eta a}, \tag{3.42}$$

as expected.

More generally, it is far easier in light scattering, particle tracking, or other experiments to measure the statistical *displacement* of the particles over time using the relation

$$\langle \hat{V}(s) V(0) \rangle = \frac{1}{2} s^2 \langle \Delta \hat{x}^2(s) \rangle. \tag{3.43}$$

If eqn 3.43 feels like a slight of hand, the reader is encouraged to derive this useful relation in Exercise 3.2. Equation 3.23 can thus be written in terms of the Laplace Transform of the mean-squared displacement,

$$\langle \Delta \hat{x}^2(s) \rangle = \frac{2k_B T}{s^2(\zeta_0 + sM_p)}. \tag{3.44}$$

Equation 3.43 has an analog in Fourier space, when the *unilateral* Fourier Transform (eqn 3.37) is computed:

$$\langle \tilde{V}(\omega) V(0) \rangle_u = \frac{1}{2} (i\omega)^2 \langle \Delta \tilde{x}^2(\omega) \rangle_u. \tag{3.45}$$

For a particle diffusing in a quasi-steady Newtonian fluid, the Laplace Transform can be inverted explicitly, giving

$$\langle \Delta x^2(t) \rangle = 2D_0 t - 2D_0 \frac{M_p}{\zeta_0} \left(1 - e^{-\zeta_0 t / M_p} \right), \tag{3.46}$$

where D_0 is given by eqn 3.42. Indeed, the MSD grows linearly in time for times $t \gg M_p/\zeta_0$, with diffusivity D_0. At very short times ($t \ll M_p/\zeta_0$), by contrast, the MSD evolves via

$$\langle \Delta x^2 (t \ll M_p/\zeta_0) \rangle \sim \frac{k_B T}{M_p} t^2, \tag{3.47}$$

reflecting ballistic probe motion with thermal velocity $V = \sqrt{k_B T / M_p}$. Notably, the fluid viscosity has no impact on the MSD over these extremely short times; and instead determines the time scale M_p/ζ_0 beyond which fluid rheology begins to dominate.

To successfully measure material rheology (here, fluid viscosity), measurements should focus on sufficiently low Laplace frequencies ($s \ll M_p/\zeta_0$). Under these conditions, eqn 3.44 may be simplified by neglecting the inertia of the probe ($ms \ll \zeta_0$), giving an approximate form

$$\langle \Delta \tilde{x}^2(s) \rangle \approx \frac{2k_B T}{s^2 \zeta_0}, \tag{3.48}$$

with inverse transform

$$\langle \Delta x^2(t) \rangle \approx \frac{2k_B T}{\zeta_0} t \tag{3.49}$$

for times $t > 0$. This is the famous Einstein equation, which is often written in terms of the particle diffusivity

$$\langle \Delta x^2(t) \rangle = 2D_0 t, \tag{3.50}$$

where D_0 is given by eqn 3.42. Using eqn 2.75 for the steady-translational resistance ζ_0 of a sphere in a viscous fluid gives the Stokes–Einstein formula for the particle diffusivity,

$$D_0 = \frac{k_B T}{6\pi \eta a}. \tag{3.51}$$

This calculation may be generalized to track displacements in two or three dimensions. Velocity autocorrelation functions, and mean square displacements, can be computed for each of the three dimensions in exactly the same way. One can track (and compute) each individually; alternatively, one can pose and solve the vector equivalent of eqn 3.17, and form the scalar product $\langle \mathbf{V}(t) \cdot \mathbf{V}(0) \rangle$ for the VAC and MSD. In that case, eqn 3.44 reads

$$\langle \Delta \hat{x}^2(s) \rangle = \frac{2\mathbb{D} k_B T}{s^2(\zeta_0 + sM_p)}, \tag{3.52}$$

where $\mathbb{D}$ is the number of dimensions tracked that contribute to the MSD:

$$\langle \Delta \hat{\mathbf{r}}^2(s) \rangle_{\mathbb{D}=2} = \langle \Delta \hat{x}^2(s) + \Delta \hat{y}^2(s) \rangle \tag{3.53}$$

$$\langle \Delta \hat{\mathbf{r}}^2(s) \rangle_{\mathbb{D}=3} = \langle \Delta \hat{x}^2(s) + \Delta \hat{y}^2(s) + \Delta \hat{z}^2(s) \rangle. \tag{3.54}$$

The calculation described made several restrictive assumptions: That the fluid and particle inertia were negligible, and that the resistance of the particle in the fluid has no "memory," meaning $\zeta(t-t') = \zeta_0 \delta(t-t')$. The latter assumption does not hold for the viscoelastic materials of interest to microrheologists, and the assumptions regarding particle inertia may or may not hold, depending on experimental conditions. In what follows, we will relax all of these assumptions to derive the *Generalized Stokes–Einstein Relation*, which is central to the entire endeavor. In fact, the core strategy and reasoning used in this simpler derivation will hold, with only minor modifications, for the more general case. We will start with the Generalized Einstein Relation, which represents one component (and assumption) of the GSER.

3.3 The Generalized Einstein Relation

The Einstein Relation previously derived relates a deterministic transport coefficient (the diffusivity) to the absolute temperature, which describes the stochastic fluctuations inherent in thermodynamic equilibrium. We have thus far limited our derivation to quasi-steady motion in purely viscous fluids. Here, we derive the Generalized Einstein Relation (GER) for more general viscoelastic fluids and solids. We thus assume no specific form for the resistance or memory function $\zeta(t-t')$, other than causality.

The derivation of the GER follows the approach taken in Section 3.2 for quasi-steady viscous fluids, now employing the Generalized Langevin Equation (Mason and Weitz, 1995; Kubo, 1966; Zwanzig and Bixon, 1970)

$$m\dot{\mathbf{V}}(t) = \mathbf{f}_B - \int_{-\infty}^{t} \zeta(t-t')\mathbf{V}(t')dt'. \tag{3.55}$$

The viscoelastic (and inertial) response properties of the medium are contained within $\zeta(t-t')$. The lower limit of integration, $-\infty$, represents the fact that the force exerted by the medium on the particle depends on the particle's past velocity history. Any time may be identified as an initial time ("$t = 0$"), since the system is in equilibrium.

3.3.1 Fourier Transform

Fourier-Transforming eqn 3.55 and using the convolution theorem gives

$$i\omega M_p\tilde{\mathbf{V}} = \tilde{\mathbf{f}}_B - \tilde{\zeta}\tilde{\mathbf{V}}, \tag{3.56}$$

which can be solved via

$$\tilde{\mathbf{V}}(\omega) = \frac{\tilde{\mathbf{f}}_B(\omega)}{\tilde{\zeta}(\omega) + i\omega M_p}. \tag{3.57}$$

Computing the scalar product with $\tilde{\mathbf{V}}^*(\omega')$ gives

$$\langle\tilde{\mathbf{V}}(\omega)\cdot\tilde{\mathbf{V}}^*(\omega')\rangle = \frac{\langle\tilde{\mathbf{f}}_B(\omega)\cdot\tilde{\mathbf{f}}_B^*(\omega')\rangle}{(\tilde{\zeta}(\omega) + i\omega M_p)(\tilde{\zeta}^*(\omega') - i\omega' M_p)}, \tag{3.58}$$

so that if the statistics of the random forcing $\mathbf{f}_B$ are known, the statistics of $\mathbf{V}$ can be determined.

Both viscoelasticity and inertia impart "memory" to the material, and therefore to the probe response—as evident from the convolution in eqn 3.55. The Brownian force in a quasi-steady Newtonian fluid (eqn 3.11) was proportional to the instantaneous probe resistance ζ_0 and had delta-function time correlation. Likewise, the time correlation of the Brownian force in a complex or inertial medium is proportional to the probe resistance, although it is not delta-correlated in time (Kubo *et al.*, 1990),

$$\langle \mathbf{f}_B(t) \cdot \mathbf{f}_B(t') \rangle = 2\mathbb{D} k_B T \zeta(|t-t'|). \tag{3.59}$$

The absolute value in eqn 3.59 reflects the fact that the autocorrelation function must be even in time—since either force may appear "first" in the averaging product—whereas causality requires $\zeta(t-t')$ to be zero for all $t' > t$. Here, we will take $\mathbb{D} = 3$ for simplicity, meaning $\mathbf{f}_B$ and $\mathbf{V}$ are three-dimensional vectors. We will give results for general dimensions after deriving the key results.

Fourier Transforming over both t and t' gives

$$\langle \tilde{\mathbf{f}}_B(\omega) \cdot \tilde{\mathbf{f}}_B(\omega') \rangle = 6k_B T \int e^{-i\omega(t-t')} e^{-i(\omega+\omega')t'} \zeta(|t-t'|) dt dt' \tag{3.60}$$

$$= 6k_B T \mathrm{Re}\left[\tilde{\zeta}(\omega)\right] \int e^{-i(\omega+\omega')t'} dt', \tag{3.61}$$

corresponding to

$$\langle \tilde{\mathbf{f}}_B(\omega) \cdot \tilde{\mathbf{f}}_B^*(\omega') \rangle = 12\pi k_B T \mathrm{Re}\left[\tilde{\zeta}(\omega)\right] \delta(\omega-\omega'). \tag{3.62}$$

The Brownian noise is not "white" but depends on frequency in the same way that the probe resistance $\tilde{\zeta}(\omega)$ does.

With this result, eqn 3.58 becomes

$$\langle \tilde{\mathbf{V}}(\omega) \cdot \tilde{\mathbf{V}}^*(\omega') \rangle = 12\pi k_B T \frac{\mathrm{Re}\left[\tilde{\zeta}(\omega)\right] \delta(\omega-\omega')}{|\tilde{\zeta}(\omega)|^2 + \omega^2 M_p^2}. \tag{3.63}$$

Inverting the Fourier Transform over ω', at a time $t' = 0$, gives

$$\langle \tilde{\mathbf{V}}(\omega) \cdot \mathbf{V}(0) \rangle = 6k_B T \frac{\mathrm{Re}\left[\tilde{\zeta}(\omega)\right]}{|\tilde{\zeta}(\omega)|^2 + \omega^2 M_p^2}, \tag{3.64}$$

so that

$$\langle \mathbf{V}(t) \cdot \mathbf{V}(0) \rangle = \frac{3k_B T}{2\pi} \int_{-\infty}^{\infty} \frac{e^{i\omega t}}{\tilde{\zeta}(\omega) + i\omega M_p} + \frac{e^{i\omega t}}{\tilde{\zeta}^*(\omega) - i\omega M_p} d\omega. \tag{3.65}$$

The two terms are non-zero for $t < 0$ and $t > 0$, respectively, because causality requires $\zeta(t < 0) = 0$, which in turn requires that ζ be analytic in the lower-half plane. The result for $t > 0$ is thus

$$\langle \mathbf{V}(t > 0) \cdot \mathbf{V}(0) \rangle = \frac{3k_B T}{2\pi} \int_{-\infty}^{\infty} \frac{e^{i\omega t}}{\tilde{\zeta}(\omega) + i\omega M_p} d\omega, \tag{3.66}$$

whereas for $t < 0$, integration over the first term vanishes to leave

$$\langle \mathbf{V}(t < 0) \cdot \mathbf{V}(0) \rangle = \frac{3k_B T}{2\pi} \int_{-\infty}^{\infty} \frac{e^{i\omega t}}{\tilde{\zeta}^*(\omega) + i\omega M_p} d\omega. \tag{3.67}$$

The $t < 0$ result can can be put in the same form as the $t > 0$ result (eqn 3.66) under the coordinate substitution $\omega \to -\omega'$,

$$\langle \mathbf{V}(t < 0) \cdot \mathbf{V}(0) \rangle = \frac{3k_B T}{2\pi} \int_{-\infty}^{\infty} \frac{e^{i\omega' |t|}}{\tilde{\zeta}(\omega') + i\omega' M_p} d\omega'. \tag{3.68}$$

In fact, both can be represented via

$$\langle \mathbf{V}(t) \cdot \mathbf{V}(0) \rangle = \frac{3k_B T}{2\pi} \int_{-\infty}^{\infty} \frac{e^{i\omega |t|}}{\tilde{\zeta}(\omega) + i\omega M_p} d\omega, \tag{3.69}$$

as one might expect from the fact that the VAC is an even function of time. When tracking dislacements in $\mathbb{D}$ dimensions, this expression becomes

$$\langle \mathbf{V}(t) \cdot \mathbf{V}(0) \rangle = \frac{\mathbb{D}k_B T}{2\pi} \int_{-\infty}^{\infty} \frac{e^{i\omega |t|}}{\tilde{\zeta}(\omega) + i\omega M_p} d\omega. \tag{3.70}$$

There are thus two ways to express the VAC in Fourier space. The *bilateral* Fourier Transform, where the time integration is performed over $-\infty < t < \infty$, is represented by eqn 3.64. Because $\langle \mathbf{V}(t) \cdot \mathbf{V}(0) \rangle$ is even in time, however, the unilateral Fourier Transform (eqn 3.37), which integrates only over positive times $0 \leq t \leq \infty$, contains identical information, and gives

$$\langle \tilde{\mathbf{V}}(\omega) \cdot \mathbf{V}(0) \rangle_u = \frac{3k_B T}{\tilde{\zeta}(\omega) + i\omega M_p} = \frac{\mathbb{D}k_B T}{\tilde{\zeta}(\omega) + i\omega M_p}. \tag{3.71}$$

The unilateral Fourier Transform and the Laplace Transform are intimately related via analytic continuation. Indeed, substituting $\omega \to -is$ into eqn 3.71 yields the Laplace Transform-derived analog (eqn

3.83). The bilateral Fourier Transform, on the other hand, can be obtained from the unilateral transform via

$$\langle \tilde{\mathbf{V}}(\omega) \cdot \mathbf{V}(0) \rangle = 2\mathrm{Re}\langle \tilde{\mathbf{V}}(\omega) \cdot \mathbf{V}(0) \rangle_u. \tag{3.72}$$

Finally, the VAC can be related to the MSD using eqn 3.45,

$$\langle \tilde{\mathbf{V}}(\omega) \cdot \mathbf{V}(0) \rangle_u = -\frac{1}{2}\omega^2 \langle \Delta\tilde{\mathbf{r}}^2(\omega) \rangle_u, \tag{3.73}$$

to give the Generalized Einstein Relation (GSER),

$$\langle \Delta\tilde{\mathbf{r}}^2(\omega) \rangle_u = \frac{6k_BT}{(i\omega)^2(\tilde{\zeta}(\omega) + i\omega M_p)}. \tag{3.74}$$

when displacements in all three dimensions contribute to $\Delta\tilde{r}^2$, or

$$\langle \Delta\tilde{\mathbf{r}}^2(\omega) \rangle_u = \frac{2\mathbb{D}k_BT}{(i\omega)^2(\tilde{\zeta}(\omega) + i\omega M_p)} \tag{3.75}$$

when displacements are tracked in $\mathbb{D}$ dimensions.

3.3.2 Laplace Transform

As written, eqn 3.55 integrates over times reaching back to $t = -\infty$, introducing problems for the Laplace Transform approach. In principle, doing so gives

$$sM_p\hat{\mathbf{V}}(s) - M_p\mathbf{V}(0) = \hat{\mathbf{f}}_B(s) - \hat{\zeta}(s)\hat{\mathbf{V}}(s) - \int_{-\infty}^{0} \mathscr{L}\{\zeta(t-t')\}\mathbf{V}(t')dt'. \tag{3.76}$$

Because $\mathbf{V}(t' < 0)$ falls outside the realm of the Laplace Transform, one cannot neatly solve for $\hat{\mathbf{V}}(s)$. This issue did not arise in eqn 3.20, because of the instantaneous response of the probe.

A common and appealing approach is to effectively ignore times $t' < 0$ in eqn 3.55,

$$M_p\dot{\mathbf{V}}(t) = \mathbf{f}_B^0(t) - \int_0^t \zeta(t-t')\mathbf{V}(t')dt', \tag{3.77}$$

and then follow the logic of Section 3.2.1. This is problematic though. After all, any probe in thermal equilibrium at $t = 0$ is nonetheless responding (statistically) to the probe's previous velocity history, due to the material's memory, be it inertial or viscoelastic. The Brownian forces $\mathbf{f}_B^0(t)$ in this approach, then, must differ from those in the stationary system (which can not depend on any particular $t = 0$).

In fact, eqn 3.77 can be viewed as an alternate version of eqn 3.55, wherein the Brownian force $\mathbf{f}_B^0(t)$ incudes "memories" of times $t < 0$, above and beyond the stationary Brownian force $\mathbf{f}_B(t)$,

$$\mathbf{f}_B^0(t) = \mathbf{f}_B(t) - \int_{-\infty}^{0} \zeta(t-t')\mathbf{V}(t')dt'. \tag{3.78}$$

If $\mathbf{f}_B^0(t)$ in eqn 3.77 had the same statistics as $\mathbf{f}_B(t)$ in the stationary distribution eqn 3.55, then eqn 3.77 would represent a sphere (and material) that was *at rest* for $t < 0$, rather than in equilibrium, and then released to start moving thermally for $t > 0$. As written, $\mathbf{f}_B^0(t)$ is therefore not stationary—it depends on time relative to "initial" time $t = 0$, at which point the system is in equilibrium, and therefore reflects memory of the statistical forces and velocities that preceded the time (arbitrarily) identified as $t = 0$.

Taking the Laplace Transform of (3.77) and using the convolution theorem yields

$$sM_p\hat{\mathbf{V}}(s) - M_p\mathbf{V}(0) = \hat{\mathbf{f}}_B^0(s) - \hat{\zeta}(s)\hat{\mathbf{V}}(s). \tag{3.79}$$

Solving for $\hat{\mathbf{V}}(s)$, taking the scalar product with $\mathbf{V}(0)$, and ensemble averaging gives the velocity correlation function

$$\langle\hat{\mathbf{V}}(s)\cdot\mathbf{V}(0)\rangle = \langle\hat{\mathbf{f}}_B^0(s)\cdot\mathbf{V}(0)\rangle + \frac{M_p\langle\mathbf{V}(0)\cdot\mathbf{V}(0)\rangle}{\hat{\zeta}(s)+sM_p}. \tag{3.80}$$

Irrespective of the viscoelastic properties of the medium, the equipartition theorem requires

$$\frac{1}{2}M_p\langle\mathbf{V}(0)\cdot\mathbf{V}(0)\rangle = \frac{\mathbb{D}}{2}k_BT, \tag{3.81}$$

reflecting the $\mathbb{D}$ translational degrees of freedom, leading to

$$\langle\hat{\mathbf{V}}(s)\cdot\mathbf{V}(0)\rangle = \langle\hat{\mathbf{f}}_B^0(s)\cdot\mathbf{V}(0)\rangle + \frac{\mathbb{D}k_BT}{\hat{\zeta}(s)+sM_p}. \tag{3.82}$$

Finally, for the distribution to be stationary, $\langle\hat{\mathbf{f}}_B^0(s)\cdot\mathbf{V}(0)\rangle$ must vanish, as was assumed in the quasi-steady Newtonian case (eqn 3.10), giving

$$\langle\hat{\mathbf{V}}(s)\cdot\mathbf{V}(0)\rangle = \frac{\mathbb{D}k_BT}{\hat{\zeta}(s)+sM_p}. \tag{3.83}$$

Equation 3.83 can be transformed into its Fourier analog eqn 3.71, via analytic continuation—simply replacing s with $i\omega$. Again, this is to be

expected based on the causal nature of $\zeta(t)$, and therefore its analyticity properties. Finally, the velocity correlation function can be related to the mean-squared displacement by invoking eqn 3.43, giving

$$\langle \Delta \hat{r}^2(s) \rangle = \frac{2\mathbb{D}k_B T}{s^2 \left[\hat{\zeta}(s) + sM_p \right]}. \tag{3.84}$$

Equation 3.84, like eqn 3.74, is called the Generalized Einstein Relation, and is central to passive microrheology. The two expressions are related by analytic continuation, effectively by substiting $s = i\omega$ (Pipkin, 1986).

These equations have the form of eqn 3.44, but the Stokes pseudo-steady-hydrodynamic resistance $\zeta = 6\pi a\eta$ has been replaced by a frequency-dependent memory function. In section 3.4, we will relate $\tilde{\zeta}(\omega)$ to the viscoelastic properties of the surrounding medium, just as ζ is related to the (frequency-independent) viscosity in the more limited case of a particle suspended in a Newtonian fluid.

Before moving on, ponder a key assumption made in this section—equipartition of energy. Equipartition only holds for systems—probe particles and their surrounding materials—that are in thermal equilibrium. This has important implications that we will consider later when discussing the limitations of passive microrheology. In particular, a probe particle in thermal equilibrium with its surroundings *cannot drive the material out of equilibrium*. Passive microrheology is therefore limited to measurements of a material's *linear* rheological response.

Another implication is that the material must not be *driven* by some out-of-equilibrium process—for instance, by swimming bacteria, the action of molecular motors or some other chemical process. Such **active matter**—including living cells—have long been studied using tracer particle methods, but their rheology cannot be measured using passive microrheology alone. For example, Mizuno *et al.* (2007) used a combination of passive and active microrheology methods to study the violation of the fluctuation dissipation theory that occurs when myosin molecular motors perform work on F-actin filament networks, further discussed in Section 7.2.1. The myosin in this case causes relative sliding of the filaments as the protein hydrolyzes ATP. In the absence of ATP, the actin-myosin network is at equilibrium, and the fluctuation dissipation-theorem is restored.

3.4 The Stokes component

In Section 3.3, we derived the Einstein component of the GSER, which relates the (measurable) mean-square displacement of a probe

particle to the resistance $\tilde{\zeta}(\omega)$ (or $\hat{\zeta}(s)$ in Laplace space) and inertia $iM_p\omega$ (or $M_p s$) of the probe as it moves in the fluid. The Einstein component thus relates a stochastic, thermally fluctuating quantity to deterministic, mechanical quantities that depend on the probe and the material. To then extract intrinsic material properties requires the probe resistance to be related the linear viscoelastic reponse properties of the material. This step comprises the "Generalized Stokes" component of the GSER.

In the Fourier domain, the frequency-dependent resistance $\tilde{\zeta}(\omega)$ gives the force exerted on the probe by the surrounding material when the probe is forced to move with oscillatory velocity at frequency ω. To actually determine $\tilde{\zeta}(\omega)$ for a material with unknown rheological properties would generally require the equations of motion for the material, in reponse to the oscillating probe. This seems at first to present a conundrum: How can one even write down—much less solve—this mechanics problem, if one does not even know the constitutive equations of the material?

The resolution to this paradox was discussed in Chapter 2. The *Correspondence Principle*, discussed in Section 2.4, demonstrates that the resistance of a spherical probe moving quasi-steadily in an incompressible Newtonian viscous fluid

$$\zeta = 6\pi a\eta, \tag{3.85}$$

yields an identical problem—and solution—in the frequency domain for an incompressible viscoelastic medium, such that

$$\tilde{\zeta}(\omega) = 6\pi a\eta^*(\omega), \tag{3.86}$$

or, by analytic continuation,

$$\hat{\zeta}(s) = 6\pi a\hat{\eta}(s). \tag{3.87}$$

Written in terms of the shear modulus, $G^*(\omega) = i\omega\eta^*(\omega)$, the quasi-steady resistance becomes

$$\tilde{\zeta}(\omega) = 6\pi aG^*(\omega)/i\omega. \tag{3.88}$$

These equations hold in the case where the fluid inertia is negligible. For Newtownian fluids, the oscillatory boundary layer thickness $\lambda_V = \sqrt{2\eta/\rho\omega}$ must be significantly larger than the probe radius a for the quasi-steady Stokes equations to be appropriate. Some tracer particle microrheology experiments, especially those employing light scattering, may approach frequencies where particle and fluid inertia cannot be neglected.

At higher frequencies, the unsteady Newtonian resistance (eqn 2.103),

$$\tilde{\zeta}(\omega) = 6\pi\eta a\left(1 + \frac{a}{\lambda_V} + i\left[\frac{a}{\lambda_V} + \frac{2a^2}{9\lambda_V^2}\right]\right) \tag{3.89}$$

can be generalized for incompressible, linear viscoelastic materials, by replacing the Newtonian viscosity η with the frequency-dependent complex viscosity $\eta^*(\omega)$ of the linear viscoelastic material, via

$$\tilde{\zeta}(\omega) = 6\pi\eta^*(\omega)a\left(1 + a(1+i)\sqrt{\frac{\rho_f\omega}{2\eta^*(\omega)}}\right) + i\omega M_f, \tag{3.90}$$

where $M_f = 2\pi\rho_f a^3/3$ is the "added mass" of the surrounding material, which oscillates along with the probe, as discussed in Section 2.5.3. We discuss the effect of inertia in microrheology experiments further in Chapter 5.

3.5 The Generalized Stokes–Einstein Relation (GSER)

Combining the results of Sections 3.3 and 3.4 yields

$$\langle\Delta\tilde{\mathbf{r}}^2(\omega)\rangle_u = \frac{-2\mathbb{D}k_BT}{6\pi\eta^*(\omega)\omega^2 a\left(1 + a(1+i)\sqrt{\frac{\rho_f\omega}{2\eta^*(\omega)}}\right) + i(M_p + M_f)\omega^3}, \tag{3.91}$$

which expresses the (experimentally-measurable) MSD entirely in terms of material properties (density and complex viscosity), frequency, probe size, and the number $\mathbb{D}$ of dimensions that are tracked and that contribute to the MSD $\langle\Delta\tilde{\mathbf{r}}^2(\omega)\rangle$. Perhaps the most important result for microrheology emerges for frequencies that are low enough for inertia to be negligible, in which case eqn 3.91 reduces to

$$\langle\Delta\tilde{\mathbf{r}}^2(\omega)\rangle_u = \frac{\mathbb{D}k_BT}{3\pi a(i\omega)^2\eta^*(\omega)}, \tag{3.92}$$

or its analog in Laplace space,

$$\langle\Delta\tilde{r}^2(s)\rangle = \frac{\mathbb{D}k_BT}{3\pi as^2\tilde{\eta}(s)}. \tag{3.93}$$

Equations 3.92 and 3.93 are generally called the Generalized Stokes–Einstein Relation, or GSER. Strictly speaking, they hold only at

frequencies low enough for inertia to be neglected. Nonetheless, this frequency range is typically broader than would be accessable to macroscopic rheometers, and therefore encompasses many frequencies of interest for soft materials. In short, this limit of the GSER connects the measured MSD of probe particles to the linear viscoelastic spectrum of the surrounding material.

Following the seminal work of Mason and Weitz (1995), eqn 3.93 was sometimes incorrectly treated as fortuitous. Soon after, however, Schnurr *et al.* (1997) essentially invoked the Correspondence Principle to rationalize why the GSER should hold for all (non-inertial) frequencies. Their correction to this sometimes persistent misunderstanding was subtle and was later reiterated clearly by Indei *et al.* (2012*b*).

Alternative forms of the GSER may be derived from eqn 3.92. Relating $\eta^*(\omega)$ to the complex shear modulus $G^*(\omega)$ via

$$G^*(\omega) = i\omega\eta^*(\omega) \tag{3.94}$$

gives an expression that may be solved for $G^*(\omega)$,

$$G^*(\omega) = \frac{\mathbb{D}k_BT}{3\pi a(i\omega)\langle\Delta\tilde{r}^2(\omega)\rangle} \tag{3.95}$$

or alternately,

$$\hat{G}(s) = \frac{\mathbb{D}k_BT}{3\pi as\langle\Delta\hat{r}^2(s)\rangle}, \tag{3.96}$$

where $\hat{G}(s)$ is the Laplace Transform of the memory function $M_r(t)$.

One can not invert these transforms exactly for generic functional forms of $G^*(\omega)$, because transformed functions appear in denominators. These relations may be inverted to give real-time relations, however, by using eqn 1.39,

$$\tilde{\mathcal{J}}(\omega) = \frac{1}{i\omega G^*(\omega)}, \tag{3.97}$$

to relate $G^*(\omega)$ in eqn 3.95 to the transformed creep compliance $\tilde{\mathcal{J}}(\omega)$,

$$\tilde{\mathcal{J}}(\omega) = \frac{3\pi a}{\mathbb{D}k_BT}\langle\Delta\tilde{r}^2(\omega)\rangle. \tag{3.98}$$

This form of the GSER may be immediately inverted (Xu *et al.*, 1998*a*; Mason, 2000), thereby connecting the measured MSD directly to the creep compliance $\mathcal{J}(t)$.

$$\mathcal{J}(t) = \frac{3\pi a}{\mathbb{D}k_BT}\langle\Delta\mathbf{r}^2(t)\rangle, \tag{3.99}$$

where $\mathbb{D}$ is the number of dimensions tracked in the experiment. Recall, the creep compliance contains the same rheological information (*i.e.*, the entire linear viscoelastic spectrum of the material).

Equation 3.99 is important. First, it reveals that it is not necessary to convert passive microrheology data to the frequency domain, despite the widespread adoption of this approach. In fact, such conversions may even introduce numerical artifacts, owing to the limited sampling range in the time domain. The methods of such conversions are discussed in Section 3.8. Second, eqn 3.99 reveals an interesting physical insight—the mean-squared displacement can be understood as a creep experiment. The mean-squared displacement of a probe particle reflects the "strain" that accumulates due to the average thermal stress imposed on the probe particle by the random Brownian force.

Equations 3.95, 3.96, and 3.99 take into account the number of dimensions tracked in a passive microrheology experiment. Measurements methods such as light scattering (Chapter 5) will report this three-dimensional value. Techniques such as multiple particle tracking (Chapter 4) will typically involve analysis of the mean-squared displacement in only one- or two-dimensional projections. It is necessary to alter eqns 3.95, 3.96, and 3.99 by the dimension, $\mathbb{D}$. For instance, data collected as a two-dimensional projection (typical for video microscopy) yields

$$\mathcal{J}(t) = \frac{3\pi a}{2k_B T}\langle \Delta r^2_{2\mathbb{D}}(t)\rangle. \tag{3.100}$$

3.6 Passive microrheology examples

Having derived the GSER—the fundamental relation that underpins passive microrheology—it is worthwhile to consider several examples of measured probe mean-squared displacements in complex and simple fluids, and how rheological properties may be determined from such data sets. Four examples are shown in Fig. 3.2.

The first example (Fig. 3.2a) shows the diffusing wave spectroscopy data of Cardinaux *et al.* (2002), wherein 0.7 and 1.5 μm diameter particles are dispersed in an aqueous surfactant solution that self-assembles into worm-like micelles (WLM). Entangled micelles form transient physical cross-links, resulting in strong viscoelastic properties. The probe motion at short delay times, far below the material's relaxation time, is sub-diffusive, reflecting the internal dynamics of the network. Over longer times, probe-particle confinement gives rise to an elastic plateau, indicating that the solution behaves like a weak viscoelastic solid. Beyond about 10^{-1} seconds,

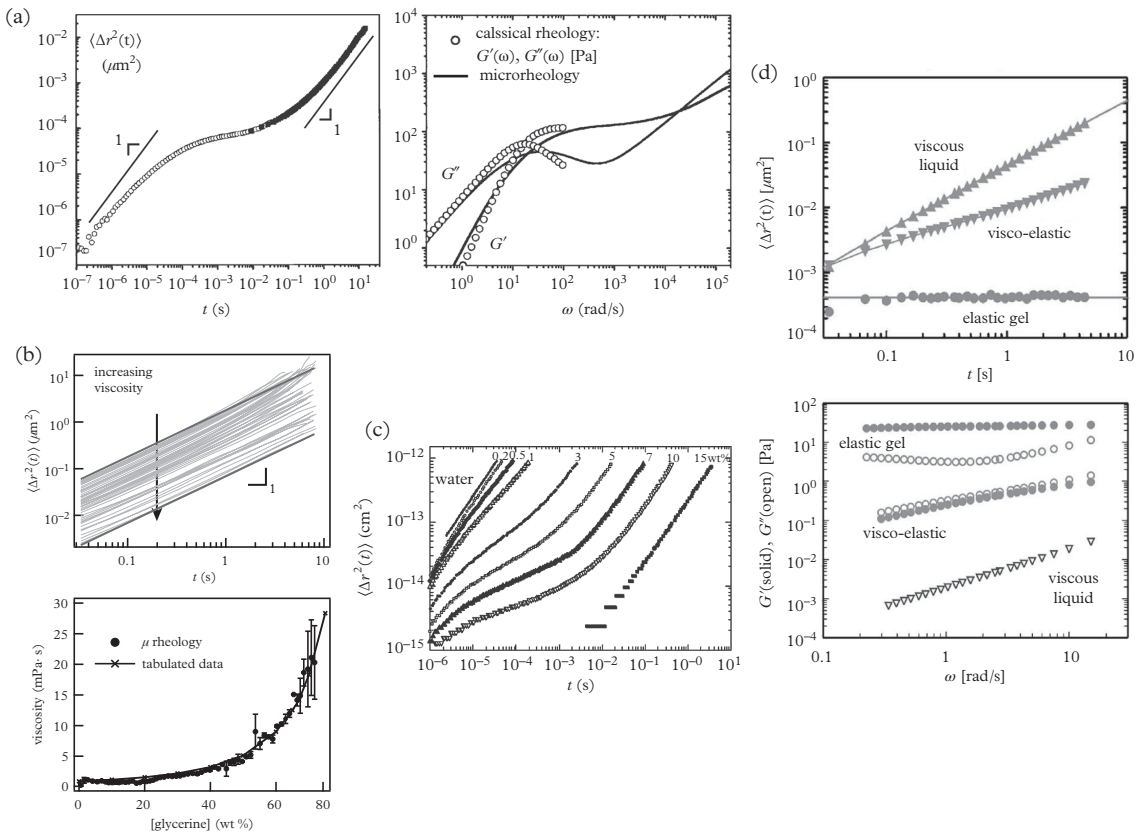

Fig. 3.2 *Examples of tracer particle dynamics in simple and complex fluids. (a) A concentrated aqueous surfactant solution that forms entangled worm-like micelles. The data is converted the to frequency domain and compared with bulk rheology measurements (Cardinaux* et al.*, 2002). Reprinted with permission from Europhys. Lett., 2002, Number 5, March, http://iopscience.iop.org/journal/0295-5075 (b) A glycerine solution with increasing viscosity. Adapted from Schultz and Furst (2011) with permission from The Royal Society of Chemistry. (c) Microrheology of PEO solutions in water. Reprinted with permission from van Zanten, J. H., Amin, S., & Abdala, A. A. Macromolelcules 37, 3874–80. Copyright (2004) American Chemical Society. (d) Alginate microrheology as the polysaccharide is induced to gel by the addition of calcium chloride. Reprinted with permission from Sato, J. & Breedveld, V.* J. Rheol.*, 50, 1–19 (2006). Copyright (2006), The Society of Rheology.*

the qualitative properties change once again, showing predominantly viscous behavior, as the WLM network relaxes and flows.

Converting the MSD results to frequency-dependent viscoelastic moduli, using methods discussed in Section 3.8, enables direct comparisons to bulk rheology measurements of the same sample, as shown in Fig. 3.2b. Notably, microrheology extends the rheology measurements to considerably higher frequencies—well into the terminal relaxation regime corresponding to the relaxation of

individual filaments. Such high-frequency data allows the stiffness of these and other supramolecular assemblies and macromolecules to be characterized, as discussed in Chapter 5.

Figure 3.2b shows the measurements of Schultz and Furst (2011) on simpler samples: Mixtures of glycerine and water for glycerine concentrations up to roughly 75 wt%. Because the mixtures are Newtonian, each MSD is simply a straight line. These measurements were made using particle tracking microrheology (Chapter 4) with microfluidic devices that are used to prepare many samples simultaneously. The viscosities, calculated by the GSER (which reduces to the Stokes–Einstein relation in this case) track the expected viscosity of these fluids.

The third example, Fig. 3.2c, is taken from van Zanten *et al.* (2004), who measured the dynamics of tracer probes in solutions of 333,000 g/mol polyethyele oxide (PEO), again with diffusing wave spectroscopy. As the polymer concentration increases from 0.2 to 10 wt%, the mean-squared displacement initially decreases as the solution viscosity increases. A significant sub-diffusive regime emerges at imtermediate concentrations, ultimately crossing over to normal diffusion.

Our last example (Fig. 3.2d) comes from multiple particle tracking measurements of alginate solutions Sato and Breedveld (2006). Here, the viscous solutions gel as salt is introduced into the sample through a dialysis membrane. At equilibrium, before and after the introduction of the salt, the mean-squared displacement curves are diffusive (viscous liquid) or entirely flat (elastic solid). Transient viscoelastic behavior is captured too, and lies in between the terminal states. In this case, particular particle-tracking microrheology captures the gelation of soft materials, an application we discuss in detail in Chapter 10.

3.6.1 Limiting behavior of the MSD

It is useful to keep in mind the limiting behavior of the mean-squared displacement that results from the GSER. In each example shown in Fig. 3.2, the mean-squared displacement is bound between that of a viscous Newtonian fluid, in which the mean-squared displacement is *linear* with time, and that of an elastic solid, which exhibits a constant, time-independent displacement. These limits will hold for for several model fluids discussed in the next section and are represented by the black curves in Fig. 3.3—one for a fluid with viscosity with a Newtonian viscosity $\eta = 1$ mPa·s and the other for an elastic solid with a modulus $G = 10$ Pa. Note that the logarithmic slope of the MSD, defined by

$$\alpha(t) = \frac{d \ln \langle \Delta r^2(t) \rangle}{d \ln t} \tag{3.101}$$

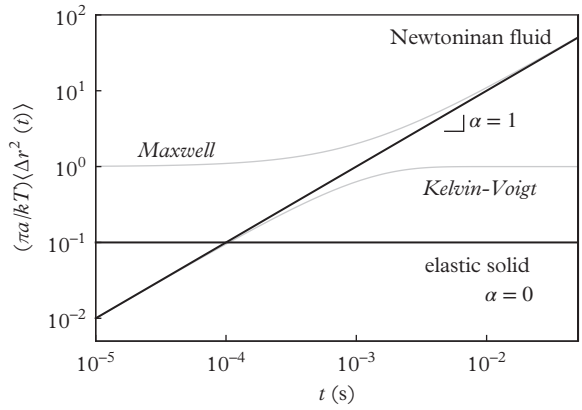

Fig. 3.3 *Limiting behavior of the MSD scaled by particle radius a and thermal energy k_BT for a Newtonian fluid with viscosity $\eta = 1$ mPa·s and elastic solid with modulus 10 Pa. A Maxwell fluid and the Kelvin-Voigt model are shown as gray lines. Both have a viscosity $\eta = 1$ mPa·s and elastic modulus $G = 1$Pa, giving identical relaxation times $\tau = \eta/G = 10^{-3}$s.*

can only have values between

$$0 \leq \alpha \leq 1. \tag{3.102}$$

Logarithmic slopes outside of this range typically indicate a problem has occurred with the passive microrheology measurement, due for instance to statistical noise of the MSD or physical sources of error, such as convection in the sample or vibration. In Section 3.8, we will show that α is related to the loss tangent, $\tan\delta(\omega) = G''(\omega)/G'(\omega)$.

3.7 GSER for model materials

We consider here the moduli and compliances for several models of viscoelastic fluids and solids and the resulting GSER equations—the creep compliance expressed as the mean-squared displacement of tracer particles. Representations of the frequency-dependent moduli and mean-squared displacement are shown in Figs 3.4, 3.5, and 3.6. This discussion should help us interpret passive microrheology results in the time domain of the experiment, rather than relying on a conversion to the frequency domain. Common methods for converting between the two domains are discussed in Section 3.8.

3.7.1 Elastic solid

An incompressible elastic solid with shear modulus $G^*(\omega) = G$, which is a real, constant quantity, and compliance

$$\mathcal{J}(t) = \frac{1}{G} \tag{3.103}$$

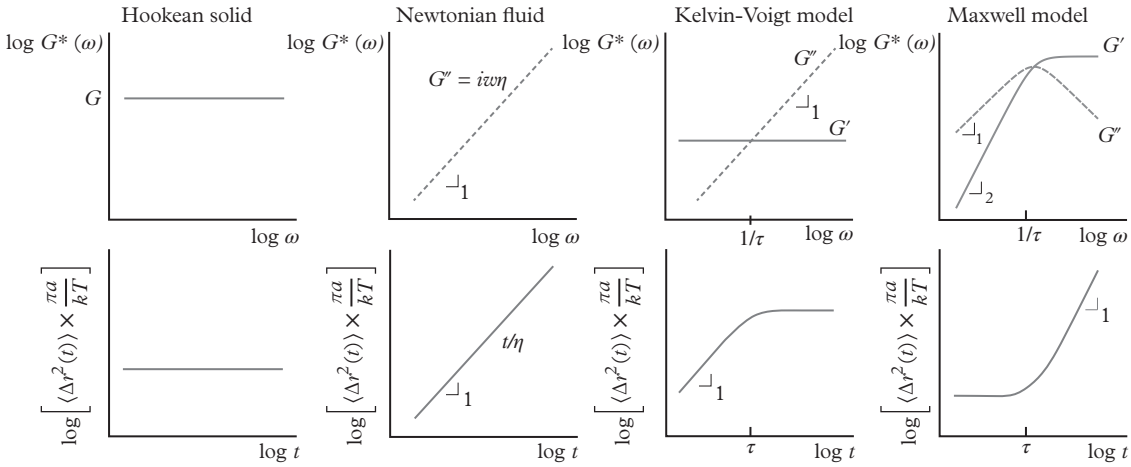

Fig. 3.4 *Schematic representations of the frequency-domain viscoelastic moduli of several model materials and the corresponding scaled mean-squared displacement (or creep compliance) from the GSER. From left to right: A Hookean elastic solid, a Newtonian fluid, the Kelvin–Voigt model (viscoelastic solid), and the Maxwell model (viscoelastic liquid). Both axes of each plot are logarithmic scales.*

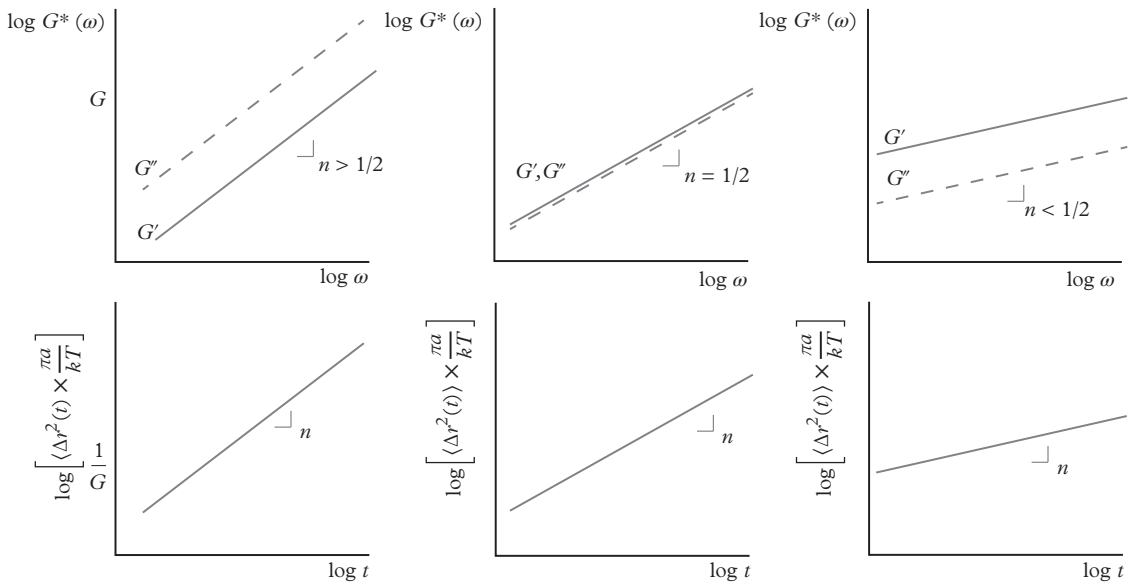

Fig. 3.5 *Schematic representations of the frequency domain viscoelastic moduli of a power-law material and the corresponding scaled mean-squared displacements (or creep compliances) from the GSER for power-law exponents $n > 1/2$, $n = 1/2$, and $n < 1/2$. Both axes of each plot are logarithmic scales.*

will exhibit a mean-squared displacement that is independent of time,

$$\langle \Delta r^2(t) \rangle = \frac{\mathbb{D} k_B T}{3\pi a G}. \tag{3.104}$$

A stiff material, with a large modulus G will have a correspondingly low compliance.

3.7.2 Viscous fluid

A Newtonian-fluid viscosity η has a creep relaxation

$$\mathcal{J}(t) = t/\eta \tag{3.105}$$

and corresponding mean-squared displacement

$$\langle \Delta r^2(t) \rangle = \frac{\mathbb{D} k_B T}{3\pi a \eta} t. \tag{3.106}$$

This is simply the Stokes–Einstein relation, eqn 3.49, with the Stokes resistance $\zeta = 6\pi a\eta$. In the frequency domain, the complex modulus is purely imaginary

$$G^*(\omega) = i\omega\eta. \tag{3.107}$$

Only the loss modulus G'' is non-zero. An increasing viscosity gives rise to a higher loss modulus, but a *lower* compliance.

3.7.3 Kelvin–Voigt model

The Kelvin–Voigt model, with frequency-dependent complex modulus

$$G^*(\omega) = G(1 + i\omega\tau), \tag{3.108}$$

or in Laplace space

$$G(s) = G(1 + s\tau), \tag{3.109}$$

describes a simple viscoelastic solid with constant storage modulus $G'(\omega) = G$, viscosity $G''(\omega) = i\omega\eta$ and characteristic relaxation time $\tau = \eta/G$.

Inverting eqn 3.98 gives

$$\langle \Delta r^2(t) \rangle = \frac{\mathbb{D} k_B T}{3\pi a G}(1 - e^{-t/\tau}). \tag{3.110}$$

The equivalent MSD expression can be found using Eqn 3.99 and the creep compliance of the Kelvin–Voigt model, as shown in Fig. 3.4,

$$\mathcal{J}(t) = \mathcal{J}(1 - e^{-t/\tau}) \tag{3.111}$$

noting that the recoverable compliance is $\mathcal{J} = 1/G$.

3.7.4 Maxwell fluid

The Maxwell fluid represents a simple model for a viscoelastic fluid, with an elastic modulus at short times and viscous relaxation at long times. Its creep compliance is (Ferry, 1980)

$$\mathcal{J}(t) = 1/G + t/\eta, \tag{3.112}$$

where $\mathcal{J} = 1/G$ is the recoverable elastic compliance. The Maxwell fluid has a complex modulus

$$G^*(\omega) = \frac{Gi\omega\tau}{1 + i\omega\tau} \tag{3.113}$$

or

$$\hat{G}(s) = \frac{Gs\tau}{1 + s\tau} \tag{3.114}$$

where

$$\tau = \frac{\eta}{G} \tag{3.115}$$

is the characteristic relaxation time of the Maxwell fluid. Expanding eqn 3.113 by multiplying $(1 - i\omega\tau)/(1 - i\omega\tau)$, we write the storage modulus

$$G'(\omega) = \frac{G\omega^2\tau^2}{1 + \omega^2\tau^2} \tag{3.116}$$

and loss modulus

$$G''(\omega) = \frac{G\omega\tau}{1 + \omega^2\tau^2}. \tag{3.117}$$

Equation 3.99 gives the mean-squared displacement for the Maxwell model,

$$\langle \Delta r^2(t) \rangle = \frac{\mathbb{D}k_BT}{3\pi aG}\left(\frac{t}{\tau} + 1\right). \tag{3.118}$$

An unusual feature of the Maxwell model at short times is that the mean-squared displacement approaches a constant value given by the elasticity of the material. Of course, a plateau in the MSD below the relaxation time $t < \tau$ is expected, but at short enough times, the probe displacement must go to zero. This apparent contradiction is an artifact of neglecting the fluid inertia in the Stokes equation, and can be corrected by properly accounting for the time-dependent equations of motion (Grimm *et al.*, 2011; Indei *et al.*, 2012*b*). We discuss inertial corrections in Section 5.6.2 when we present high-frequency microrheology with diffusing wave spectroscopy.

3.7.5 Power-law response

A material with a power-law response has a shear relaxation modulus

$$G(t) = Kt^{-n} \tag{3.119}$$

where K, the "consistency" has fractional units Pa·s^n and n is an exponent bounded by $0 < n < 1$. Then the storage and loss moduli scale as $G' \sim G'' \sim \omega^n$ over all frequencies (Winter and Mours, 1997; Jaishankar and McKinley, 2012). Specifically,

$$G^*(\omega) = K\Gamma(1-n)(i\omega)^n \tag{3.120}$$

and

$$G'(\omega) = K\Gamma(1-n)\omega^n \cos\frac{n\pi}{2} \tag{3.121}$$

$$G''(\omega) = K\Gamma(1-n)\omega^n \sin\frac{n\pi}{2} \tag{3.122}$$

where $\Gamma(x)$ is the gamma function. Whether the material response is dominated by viscous or elastic behavior depends on the value of n: For $n > 1/2$ the loss modulus has larger magnitude than the storage modulus. When $n < 1/2$, the storage modulus has larger magnitude than the loss modulus. When $n = 1/2$, neither dominates, meaning that $G' = G''$ over all frequencies.

Power-law rheology arises when a hierarchy of relaxation time scales are established by a microstructure that is self-similar over a wide range of length scales. An example is the fractal structure of an incipient gel at the percolation transition (Winter and Chambon, 1987; Martin *et al.*, 1988; Adolf and Martin, 1990; Winter and Mours, 1997). Power-law rheology also occurs in many complex materials and products, including biofluids, foods, cross-linked polymers, microgels, and hydrogels.

The Laplace Transform of $G(t)$ for the power law material is

$$\hat{\eta}(s) = \int_0^\infty Kt^{-n}e^{-st}dt = K\frac{\Gamma(1-n)}{s^{1-n}}, \tag{3.123}$$

where we note again that the complex viscosity and relaxation modulus are transform pairs, as discussed in Section 1.2.2.[7] The Laplace-transformed creep compliance is then given by

$$\hat{\mathcal{J}}(s) = \frac{1}{K\Gamma(1-n)}\frac{1}{s^{n+1}}, \tag{3.124}$$

with inverse

$$\mathcal{J}(t) = \frac{t^n}{K\Gamma(1-n)\Gamma(n+1)}. \tag{3.125}$$

This can be simplified using the relation $\Gamma(1-n)\Gamma(n+1) = n\pi/\sin n\pi$, giving

$$\mathcal{J}(t) = \frac{\sin n\pi}{n\pi K}t^n, \tag{3.126}$$

from which the GSER determines the mean-squared displacement to be

$$\langle \Delta r^2(t)\rangle = \frac{\mathbb{D}k_BT\sin n\pi}{3n\pi aK}t^n \tag{3.127}$$

for a probe in a power-law fluid, as shown in Fig. 3.5.

3.7.6 Rouse and Zimm models

The Rouse model is a bead-spring representation of dilute flexible polymers dispersed in a Newtonian solvent (Ferry, 1980; Doi and Edwards, 1986; Rubinstein and Colby, 2003). Beads of radius b are connected by Hookean springs. The beads represent the hydrodynamic drag exerted on the polymer chains, and the stiffness of the springs captures the entropic elasticity of the flexible molecules. The relaxation modulus is a summation over the relaxation of the chain's normal modes

$$G(t) = nk_BT\sum_{p=1}^{N} e^{-t/\tau_p}. \tag{3.128}$$

Here, n is the number density of molecules and τ_p is the characteristic relaxation time of the p^{th} mode of a chain consisting of N beads,

$$\tau_p = \frac{\zeta b^2N^2}{6\pi^2k_BTp^2} \tag{3.129}$$

[7] The literature often uses $\tilde{G}$ or $\hat{G}$ to denote transforms of the relaxation modulus. We instead use the transformed viscosity $\eta^*(\omega)$ or $\hat{\eta}(s)$, to avoid confusion with the complex modulus $G^*(\omega)$ and its Laplace variant $\hat{G}(s)$.

where the friction coefficient on each bead is $\zeta \approx \eta_s b$ and η_s is the solvent viscosity. The longest relaxation time of the polymer, corresponding to the mode $p = 1$, is

$$\tau_R = \frac{\zeta b^2 N^2}{6\pi^2 k_B T} \tag{3.130}$$

and the shortest time scale of the relaxation is that of the monomer,

$$\tau_0 \approx \frac{\zeta b^2}{k_B T}. \tag{3.131}$$

In the frequency domain, the storage and loss moduli of the Rouse model are

$$G'(\omega) = nk_B T \sum_{p=1}^{N} \frac{\omega^2 \tau_p^2}{1 + \omega^2 \tau_p^2} \tag{3.132}$$

and

$$G''(\omega) = \omega \eta_s + nk_B T \sum_{p=1}^{N} \frac{\omega \tau_p}{1 + \omega^2 \tau_p^2}, \tag{3.133}$$

representing the summation over N distinct relaxation times in the Maxwell model.

As illustrated in Fig. 3.6, Between the frequencies $1/\tau_0 < \omega < 1/\tau_R$ in the terminal regime, the Rouse model moduli scale as

$$G'(\omega) = G''(\omega) - \omega \eta_s \sim \omega^{1/2}. \tag{3.134}$$

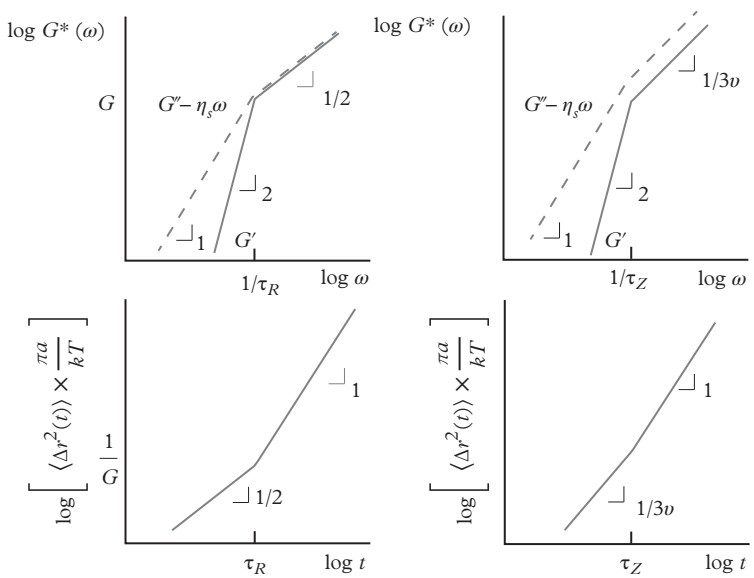

Fig. 3.6 *Schematic representations of the frequency domain viscoelastic moduli of the Rouse and Zimm models of polymer solutions and the corresponding scaled mean-squared displacements (or creep compliances) from the GSER. Both axes of each plot are logarithmic.*

That is, they are equal and have a power-law dependence on frequency of $\omega^{1/2}$—a signature of the "free-draining" hydrodynamics of the model.[8] Likewise, the creep compliance scales as $t^{1/2}$ at short times. Thus, the mean-squared displacement of a probe particle in a passive microrheology experiment will exhibit sub-diffusive motion,

$$\langle \Delta r^2(t) \rangle \sim t^{1/2} \qquad \tau_0 < t < \tau_R. \tag{3.135}$$

Below $\omega < 1/\tau_R$, $G'(\omega) \sim \omega^2$ and $G''(\omega) \sim \omega$. For $t > \tau_R$, there is a cross-over from sub-diffusive to diffusive probe dynamics, $\langle \Delta r^2(t) \rangle \sim t$.

The Zimm model differs from the Rouse model by accounting for the hydrodynamic interactions between the beads of the bead-spring model. The polymer is no longer considered "free-draining." This affects the terminal high-frequency response of the solution, which takes on a power law form

$$G'(\omega) \sim G''(\omega) - \omega\eta_s \sim \omega^{1/3\nu} \tag{3.136}$$

where the Flory exponent ν depends on the polymer-solvent interaction. In theta-solvents, $\nu = 1/2$ and the scaling becomes $G'(\omega) \sim G''(\omega) - \omega\eta_s \sim \omega^{2/3}$, while polymers in good solvents exhibit a lower Flory exponent, $\nu \approx 0.588$, and correspondingly lower exponent (~ 0.57). The terminal regime will be apparent in the mean-squared displacement at time scales shorter than the Zimm relaxation time $\tau_Z \approx \tau_0 N^{3\nu}$,

$$\langle \Delta r^2(t) \rangle \sim t^{1/3\nu} \qquad \tau_0 < t < \tau_Z. \tag{3.137}$$

3.7.7 Semiflexible polymers

Semiflexible polymers are macromolecules and macromolecular assemblies for which the degree of the polymer backbone rigidity becomes a significant source of elasticity and dissipation compared to flexible and rod-like molecules. Comprehensive models for the rheology of semiflexible polymers have been discussed by Morse (1998*c*,*a*,*b*), Shankar *et al.* (2002), MacKintosh *et al.* (1995), and Gittes and MacKintosh (1998). These theories cover a wide range of conditions, including concentration (ranging from the dilute to tightly entangled), persistence lengths (from flexible to rigid), and the effect of cross-linkers.

[8] This is different from the free-draining limit of the compressibility discussed in Chapter 2.

The rheology of semiflexible polymers has been especially prominent in the microrheology literature largely due to the number of examples that are found in biological materials, especially the protein filaments and microtubules that dominate cell and tissue mechanics (Dichtl and Sackmann, 2002; Addas *et al.*, 2004), filamentous viruses (Sarmiento-Gomez *et al.*, 2012), and peptide assemblies (Ozbas *et al.*, 2004). A hallmark of semiflexible polymer microrheology is that its high-frequency terminal response takes on the scaling

$$G^*(\omega) \sim \omega^{3/4}, \tag{3.138}$$

which means that the mean-squared displacement scales as

$$\langle \Delta r^2(t) \rangle \sim t^{3/4} \tag{3.139}$$

at short times. This scaling has been measured by microrheology using diffusing wave spectroscopy, magnetic tweezers, and laser tracking microrheology (Amblard *et al.*, 1996; Gittes *et al.*, 1997; Palmer *et al.*, 1998, 1999; Mason *et al.*, 2000). Indeed, this is one direct means of measuring the persistence length l_p of a material composed of semiflexible polymers and supramolecular assemblies, as we discuss in Section 5.6.

3.8 Converting between the time and frequency domains

In Section 3.5, we found that the shear modulus in the frequency domain can be expressed in terms of the Laplace or Fourier Transform of the mean-squared displacement. In experiments such as video microscopy particle tracking (Chapter 4) and light scattering (Chapter 5) the mean-squared displacement is measured directly as a function of real time, at discrete time intervals over a range of times. We noted that the time-domain data can be interpreted directly as a creep measurement, but it is often desirable to express the microrheology in the frequency domain to compare with oscillatory bulk rheology or theory. The widespread use of oscillatory rheology has also made interpretation of rheological measurements in the frequency domain more familiar to many rheologists.

While a direct numerical transform of the time-domain data to the frequency domain is possible, this method is often unreliable, in that it leads to significant truncation errors at the frequency extremes. Others have used polynomial fits of the logarithmic time-domain data

$\ln\langle\Delta r^2(\ln t)\rangle$ and their analytical transforms into the frequency domain (Willenbacher *et al.*, 2007). Drawbacks include the accuracy of the fit, the potential to introduce artifacts into the transformed data, and the possibility that the apparent frequency-dependent moduli do not satisfy the Kramers-Kronig relations (cf. Section 1.2.2). Two other methods for converting the time-domain data to the frequency domain include the power-law approximation and methods of constrained regularization.

3.8.1 Power-law approximation

One common method of calculating the frequency-domain moduli in microrheology is to approximate the MSD at each sampled time t_0 as a power–law function,

$$\langle\Delta r^2(t)\rangle \approx \langle\Delta r^2(t_0)\rangle(t/t_0)^{\alpha(t_0)}, \tag{3.140}$$

where $\alpha(t_0)$ is the logarithmic slope of the mean-squared displacement evaluated at t_0,

$$\alpha(t_0) = \left.\frac{d(\ln\langle\Delta r^2(t)\rangle)}{d(\ln t)}\right|_{t=t_0}. \tag{3.141}$$

The Laplace Transformation of a power-law,

$$\mathscr{L}\{t^p\} = \frac{\Gamma(p+1)}{s^{p+1}} \tag{3.142}$$

where $\Gamma(x)$ is the Gamma function, implies that

$$s\langle\tilde{\Delta} r^2(s)\rangle = \langle\Delta r^2(t_0)\rangle(s_0/s)^{\alpha(t_0)}\Gamma(\alpha+1), \tag{3.143}$$

with $s_0 = 1/t_0$. Equation 3.96 is then recovered, giving

$$G(s_0) = \left.\frac{\mathbb{D}k_BT}{3\pi a\langle\Delta r^2(t_0)\rangle\Gamma[\alpha(t_0)+1]}\right|_{t_0=1/s_0}, \tag{3.144}$$

Here again, $\mathbb{D}$ represents the number of dimensions tracked for the mean-squared displacement. Evaluating eqn 3.144 at each sampled time t_0 in the MSD gives the corresponding relaxation modulus at $s_0 = 1/t_0$ from the value of the MSD and its logarithmic slope, as illustrated in Fig. 3.7. Similarly, the Fourier domain yields the modulus amplitude,

$$|G^*(\omega_0)| = \left.\frac{\mathbb{D}k_BT}{3\pi a\langle\Delta r^2(t_0)\rangle\Gamma[\alpha(t_0)+1]}\right|_{t_0=1/\omega_0}. \tag{3.145}$$

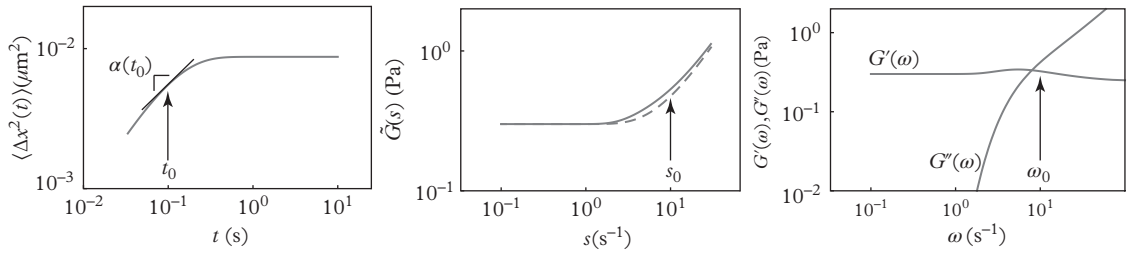

Fig. 3.7 *(Left) MSD for a Voigt model fluid. The MSD and logarithmic slope α are evaluated at* t_0. *(Middle) The corresponding* $\tilde{G}(s)$. *The dashed line is Eqn 3.144 neglecting the Gamma function. (Right) The storage (solid line) and loss (dashed line) moduli.*

From this, the storage $G'(\omega)$ and loss $G''(\omega)$ moduli are calculated as

$$G'(\omega) = |G^*(\omega)| \cos(\pi\alpha(\omega)/2) \tag{3.146}$$

$$G''(\omega) = |G^*(\omega)| \sin(\pi\alpha(\omega)/2). \tag{3.147}$$

Alternatively, the loss tangent can be expressed as

$$\tan\delta(\omega) = G''(\omega)/G'(\omega) = \tan[\pi\alpha(\omega)/2]\,. \tag{3.148}$$

This equation gives the relation between the phase angle and logarithmic slope of the mean-squared displacement,

$$\delta(\omega) = \frac{\pi}{2}\alpha(\omega). \tag{3.149}$$

With α limited to values between 0 and 1, the phase angle is constrained to $0 \le \delta \le \pi/2$. In the limit of an elastic solid, $\alpha = 0$ and $\tan\delta = 0$, and of course the loss tangent diverges for $\alpha = 1$.

The approximate transform to the frequency domain based on the power–law approximation works well when $\langle \Delta r^2(t) \rangle$ is a fairly smooth function of time (on a doubly logarithmic scale). For cases in which the MSD exhibits more curvature, higher-order terms in the power–law expansion can be included (Dasgupta *et al.*, 2002). The chief drawback of the approximate method is the accuracy of the numerical differentiation of the MSD to calculate its logarithmic slope, α. The differentiation mainly affects $\tan\delta$ or G' and G'' and not $G(s)$ or $|G^*(\omega)|$, since the Gamma function is a weak function of its permissible values, $1 \le \alpha + 1 \le 2$, as illustrated by plotting $\Gamma(x)$ for $1 \le x \le 2$ in Fig. 3.8. The calculated values of G' and G'' may also deviate significantly when the cosine and sine functions in eqns 3.146 and 3.147 approach zero. This is clearly evident in Fig. 3.7 for the low-ω behavior of G'', which decays more quickly as $\omega \to 0$ than the $G''(\omega) = \eta\omega$ allowed by the Kelvin-Voigt model.

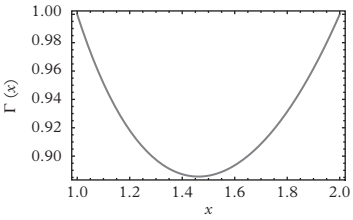

Fig. 3.8 *The Gamma function evaluated over the range of permissible values for the logarithmic MSD slope,* $1 \le \alpha + 1 \le 2$.

3.8.2 Constrained regularization

An alternate to the approximate transform is to calculate $\langle \Delta \tilde{r}^2(s) \rangle = \mathscr{L}\{\langle \Delta r^2(t) \rangle\}$ using a constrained regularization method (Honerkamp and Weese, 1989; Elster *et al.*, 1992; Honerkamp and Weese, 1993; Solomon and Lu, 2001; Lu and Solomon, 2002; Starrs and Bartlett, 2003*a*). In one version of this approach, the relaxation modulus $G(t)$ is expressed as a summation of N Maxwell model relaxation modes (Ferry, 1980; Honerkamp and Weese, 1989),

$$G(t) = \sum_{i=1}^{N} h_i e^{-t/\tau_i} \tag{3.150}$$

where h_i and τ_i are the amplitude and relaxation time of mode i, respectively.[9] The Laplace Transform of eqn 3.150 is the shear modulus

$$\hat{\eta}(s) = \sum_{i=1}^{N} \frac{h_i s\tau_i}{1 + s\tau_i}. \tag{3.151}$$

The inverse problem is to identify values of h_i and τ_i such that eqn 3.150 is a good description of the time-domain mean-squared displacement.

The number of relaxation times, their values, and their individual weighting is an ill-posed problem—the errors in the inversion are unbounded. Instead, one determines the values of h_i and τ_i using constraints that, for instance, require the relaxation spectrum to be smooth or at least continuous. Lu and Solomon (2002), for instance, use the method of Provencher (1982*a*) implemented in the program package CONTIN. They suggest that constrained regularization may perform better than the power-law approximation, as previously discussed, when the rheology exhibits a strong frequency dependence. A comparison of the CONTIN and power-law approximation methods using light-scattering microrheology for an associative polymer solution are shown in Figure 3.9. The CONTIN derived data does agree with the low-frequency response of the bulk rheometry data much more closely than the moduli calculated using the power-law approximation.

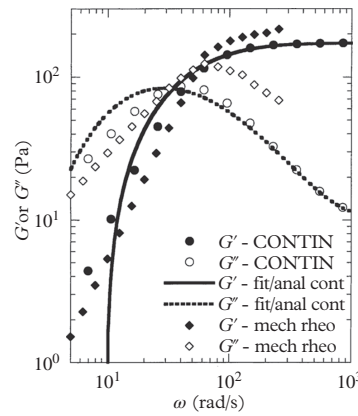

Fig. 3.9 *Microrheology of 4 wt% telechelic associative polymer thickener. Reprinted from* Curr. Opin. Colloid Interface Sci., *6, Solomon, M. J. & Lu, Q. Rheology and dynamics of particles in viscoelastic media, 430–7, Copyright (2001), with permission from Elsevier.*

Another regularization method uses the Tirkhonov regularized fit of the mean-squared displacement (or creep compliance) with a set of N basis functions derived from a Voigt fluid (Mason *et al.*, 2000; Ferry, 1980)

$$\mathscr{J}(t) = \sum_{n=1}^{N} L_n (1 - e^{-t/\tau_n}) \tag{3.152}$$

[9] This expression can be applied to viscoelastic solids by including a finite static modulus.

or Kelvin-Voigt model (Kloxin and Van Zanten, 2009; Tanner *et al.*, 2011),

$$\mathcal{J}(t) = \sum_{n=1}^{N} L_n(1 - e^{-t/\tau_n}) + \frac{t}{\eta_0}. \tag{3.153}$$

The number of terms is kept smaller than the measured data points and τ_N are fixed to be logarithmically spaced. The coefficients L_n are determined subject to the minimization of a function that weights the residual sum of squares between the fitted function and measured values $\hat{\mathcal{J}}(t)$ with a "smoothness" constraint,

$$\text{minimize: } [\mathcal{J}(t) - \hat{\mathcal{J}}(t)]^2 + \lambda \frac{\partial^2 L}{\partial \tau^2}. \tag{3.154}$$

This combination of terms prevents unphysical variations in the values of L_n. The smoothness is determined by the parameter λ and is given by the method implemented by Weese (Weese, 1993; Weese, 1992). Once an appropriate model of the retardation spectrum is found, the complex shear modulus is

$$G^*(\omega) = \left(\sum_{n=1}^{N} \frac{L_n}{1 + i\omega\tau_n} \right)^{-1}. \tag{3.155}$$

An example of the regularized fit of the Voigt fluid basis functions is shown in Fig. 3.10 for entangled semiflexible networks of F-actin. The mean-squared displacement (or creep compliance) is

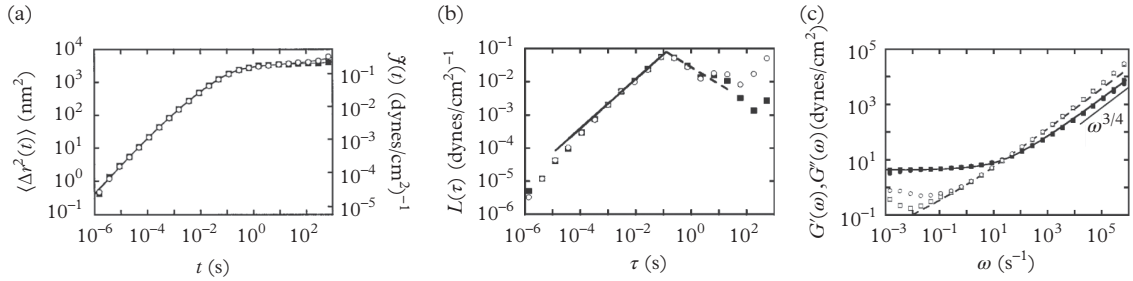

Fig. 3.10 *The microrheology of entangled F-actin solutions. (a) The mean-squared displacement of 1.6 μm diameter probes. (b) The retardation spectrum $L(\tau)$. (c) The calculated viscoelastic moduli. The solid points are the storage modulus $G'(\omega)$ and the open points are the loss modulus $G''(\omega)$. Reprinted with permission from Mason, T. G., Gisler, T., Kroy, K., Frey, E., & Weitz, D. A.* J. Rheol., *44, 917–28 (2000). Copyright (2000), The Society of Rheology.*

fit using equation 3.152 with $N = 25$ terms. The resulting retardation spectrum is given in Fig. 3.10b from which the storage and loss moduli are calculated using eqn 3.155. The Tirkhonov regularized fit method has also been used to analyze probe microrheology measurements of micellar solutions of block copolymers (Kloxin and Van Zanten, 2009; Tanner *et al.*, 2011) and associative polymers (Abdala *et al.*, 2015).

3.9 Strengths and limitations of passive microrheology

The reader is no doubt interested in the theory and practice of microrheology due to its many potential applications. The small sample size requirements of microrheology and the ease of its implementation—at minimum requiring simple movies of particle Brownian motion—are among its strengths that will be highlighted throughout the remainder of this book. However, there are several important limits on passive microrheology that can be brought to light based on the discussion in this chapter.

The first and foremost limitation of passive microrheology is that it can *only measure a material's linear rheology*, because probe particles are in thermal equilibrium with the surrounding material. A probe in equilibrium with a material may not drive that material out of equilibrium! As a result, many interesting and technologically important rheological properties are inaccessible to passive microrheology: Yielding, shear thinning, shear thickening, and so on. Such behaviors, which arise when a material is driven strongly out of equilibrium, can only accessed in microrheology by *active* techniques in which the probe motion is driven by non-thermal forces, as discussed in Chapter 7.

Second, passive microrheology is limited to materials with rather weak moduli and low viscosities (or correspondingly large compliances) compared to many bulk-rheology measurements, because it depends on thermal motion as the driving force. The average thermal stress exerted on a particle scales as $\sim k_B T/a^3$. For a one micrometer diameter particle, this is on the order of just 10^{-2} Pa. As we discuss later, this range does not necessarily limit the utility of microrheology; it can still be used to screen whether an elastic gel forms from a precursor viscous fluid, for instance, even if the compliance is too low to be measured quantitatively. Conversely, passive microrheology excels at measuring many weakly-elastic or low-viscosity materials that are otherwise difficult to characterize using bulk rheometry, especially if the material is only available in limited quantities.

3.10 Validity of the GSER

The validity of the GSER depends on how well the assumptions made in its derivation apply to the experiment at hand, the two key ones being: (1) The applicability of the Stokes equation—the probe experiences a continuum mechanical environment—and (2) that the material is at thermal equilibrium, or sufficiently close to thermal equilibrium to constitute a "quasi-equilibrium" in the case of materials undergoing a chemical reaction, such as gelation or degradation. Non-continuum effects are not limited to passive microrheology, but affect all forms of probe microrheology, including active microrheology; they are all based on the Stokes relation relating the force acting on a probe that accompanies the material deformation.

3.10.1 Non-continuum effects

For the Stokes component we can ask whether the material behaves as a continuum on the length scale of a probe particle. This assumption could be violated if the probe size is smaller than the length scales of the material microstructure, as we discussed in Section 2.2. The local microstructure can also be changed by the particle.

A number of ways have been used to experimentally verify the validity of the continuum behavior in passive microrheology. Comparing the calculated moduli to other experiments, including bulk rheology, in overlapping frequency ranges (or by extrapolating one data set to the other) is one approach to testing its validity. Another method is to perform a series of experiments using different probe sizes, and a third is to use particles with different surface chemistries. Finally, the correlated motion of probes, presented in Section 4.11 and called two-point microrheology, can be used to measure the microrheological response on length scales larger than the probe diameter.

Particle size

Measurements made with probes of several diameters should collapse when scaled by the corresponding probe radius

$$\langle \Delta r^2(t) \rangle a = \frac{\mathbb{D} k_B T}{3\pi} \mathcal{J}(t) \tag{3.156}$$

provided the GSER is satisfied. Microrheology measurements of associative polymer solutions using a range of probe particles with diameters from 0.3 to 2.0 μm provide a good illustration of one such breakdown of the GSER (Lu and Solomon, 2002). As we see in

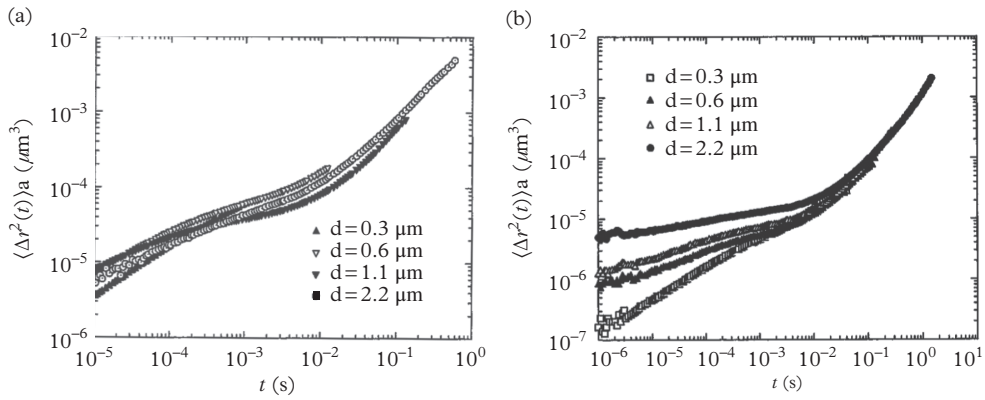

Fig. 3.11 *Microrheology of HEUR associative polymers at (a) low concentration—1 wt%, and (b) higher concentration—4 wt%. Reprinted with permission from Lu, Q. & Solomon, M.* J., Phys. Rev. E, *66, 61504 (2002) Copyright (2002) by the American Physical Society.*

Fig. 3.11a, the mean-squared displacements for probes at the lower concentration of polymer collapse when scaled by the particle radius. At a higher-polymer concentration, however, the mean-squared displacements fail to collapse at the shortest times (Fig. 3.11b). The deviation from the GSER behavior is associated with the formation of a growing network of polymers. The results suggest that larger particles are sufficiently entangled in the developing network and exhibit a plateau modulus consistent with Maxwell fluid rheology, but that smaller particles are able to percolate through the presumably inhomogeneous structure. It is also apparent in Fig. 3.11b that beyond some relaxation time of the polymer network, probes of all diameters move as if in a viscous solution, and the proper particle scaling is recovered.

Microrheology experiments by van Zanten *et al.* (2004) for aqueous poly(ethylene oxide) (PEO) solutions demonstrate the proper particle size scaling expected of the GSER. The data are reproduced in Fig. 3.12. Four experiments measuring the Brownian motion of spherical polystyrene tracers in 7 wt% PEO collapse on a single curve when plotted as the creep compliance, $\mathcal{J}(t) = (\pi a/k_B T)\langle \Delta r^2(t) \rangle$, which scales out the particle size. The four probe diameters tested range from 0.195 to 1.55 μm.

Surface chemistry

The surface chemistry of the probes can affect microrheology measurements. Such a dependence usually indicates the depletion,

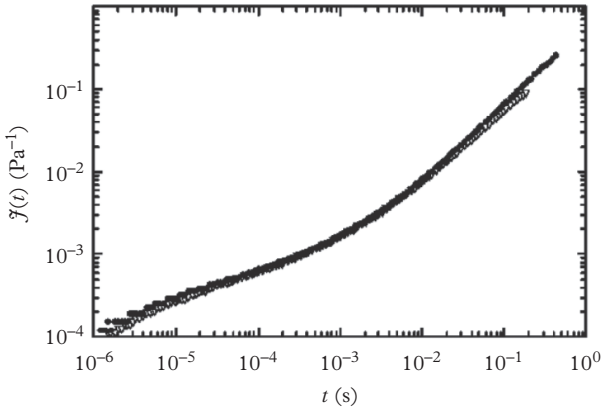

Fig. 3.12 *Microrheology of poly (ethylene oxide) polymers solutions using for probe sizes ranging from 0.195 to 1.55 μm diameter. Adapted with permission from van Zanten, J. H., Amin, S., & Abdala, A. A.* Macromolelcules *37, 3874–80 (2004). Copyright (2004) American Chemical Society.*

accumulation, or restructuring of the material in the vicinity of the probe.

A good example is the sensitivity of F-actin microrheology on probe chemistry. McGrath *et al.* (2000) used laser tracking microrheology to measure the microrheology of tightly entangled F-actin networks and found that the modulus amplitude and phase angle depended on the surface chemistry of polystyrene probes, as shown in Fig. 3.13. The modulus amplitude had a clear dependence on the capacity of the probes to adsorb F-actin monomer. Also notable is the significant difference in the phase angle, plotted in Fig. 3.13b, across the samples. Probes with the lowest binding capacity have a phase

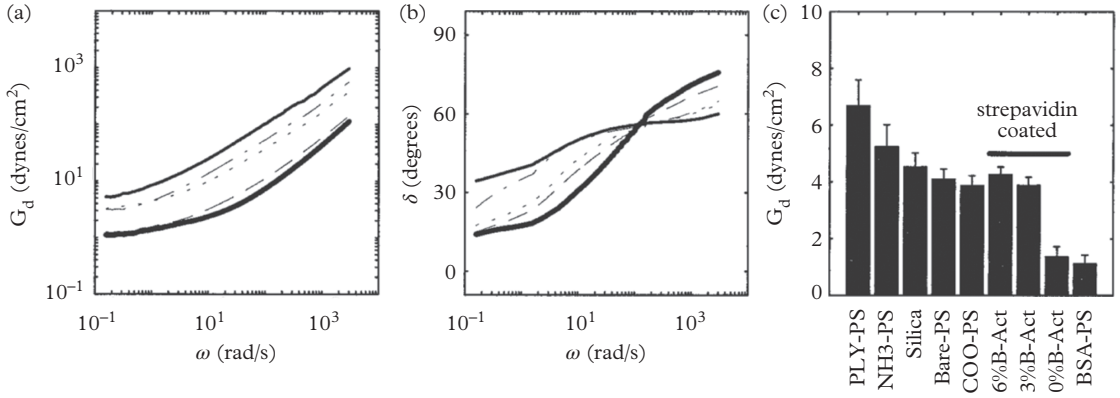

Fig. 3.13 *The dependence of F-actin microrheology on the surface chemistry of the polystyrene probes. Reprinted from* Biophys. J., *79, McGrath, J. L., Hartwig, J. H., & Kuo, S. C., The mechanics of F-actin microenvironments depend on the chemistry of probing surfaces, 3258–66, Copyright (2000), with permission from The Biophysical Society.*

angle approaching 90 degrees at high frequency, like a Newtonian fluid, probes with strong interactions to the F-actin produce phase angles consistent with the expected scaling of the semiflexible polymer high-frequency moduli, $\delta \sim 50^\circ \sim \tan^{-1}[(3/4)(\pi/2)]$.

For probes that bind weakly to the F-actin network, the measured rheology is intermediate between that which one expects for the solvent and a tightly entangled semiflexible polymer network. This behavior is an indication that a shell of softer or depleted material has formed around the probes (Levine and Lubensky, 2001), and is discussed in more detail in Section 4.11.4. Similar to depletion, a higher density of material may accumulate near the probe surface, although this will appear as an increase in the effective probe size. Microrheology measurements in this case generally produce the correct frequency response, but with an apparent modulus that is higher than the true modulus. In other cases, discrete contact points between the probes and material may occur, with depleted regions between these. The probes are expected to report the correct frequency dependence of the rheology, but with a lower apparent modulus (Van Citters *et al.*, 2006).

3.10.2 Microrheology without probes?

In the "tracer probe" microrheology that we have been considering, a material is seeded with colloidal particles. The dynamics of these particles are used to measure the microrheology. Most often these probes are particles which are added to the material of interest. However, nothing prevents us from measuring the dynamics of the material itself, for instance if it's a concentrated emulsion or colloidal suspension. Can the rheology be derived from these experiments with the GSER?

Some of the first studies using light-scattering microrheology do measure the dynamics of emulsions and suspensions (Mason and Weitz, 1995; Mason *et al.*, 1997*b*). As we can see for the dynamics of concentrated emulsions in Fig. 3.14a, the droplets exhibit a mean-squared displacement reminiscent of the Kelvin–Voigt model. In fact, the Laplace-Transformed Kelvin–Voigt model (eqn 3.109) is compared to the transformed data by the dashed line Fig. 3.14b, matching the asymptotic solid and viscous limits. The difference between the model and data are represented by the open symbols and fit the power-law function $s^{0.5}$ over about six decades. When the Kelvin–Voigt model and power-law are converted to moduli, they agree well with mechanical rheology. That comparison can be seen in Fig. 3.14c.

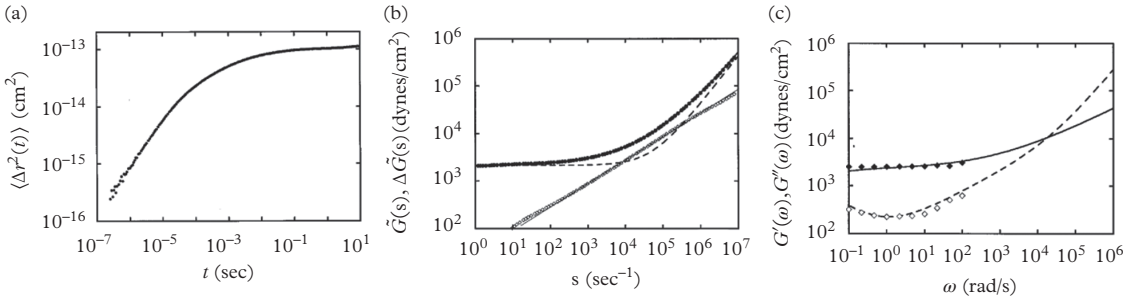

Fig. 3.14 *Dynamics of concentrated-monodisperse emulsion droplets (volume fraction $\phi = 0.65$) measured by diffusing wave spectroscopy. (a) The emulsion droplets' mean-squared displacement and (b) its Laplace Transform (solid symbols). (c) The storage and loss moduli derived from the light scattering are in good agreement with bulk rheology (symbols) in the overlapping frequency range. Adapted with permission from Mason* et al. *(1997*b*), The Optical Society.*

The agreement between bulk rheology and the rheology derived from the emulsion droplet dynamics seems to violate one of the key assumptions of our derivations in this chapter—that the medium constitutes a continuum on the length scale of the probe particle. In these cases, the probe particles are the material of interest. Earlier studies of hard-sphere suspensions, the Stokes–Einstein relation relating the short-time self-diffusivity D_s^s to the high-frequency viscosity η'_∞,

$$D_s^s(\phi) \overset{?}{\propto} \frac{\mathbb{D}k_BT}{3\pi a\eta'_\infty(\phi)}, \tag{3.157}$$

holds to within experimental accuracy across a wide range of volume fractions (Shikata and Pearson, 1993; Banchio *et al.*, 1999), but fails for dispersions in which particles interact by screened electrostatic interactions (Horn *et al.*, 2000). Such applications of the Stokes–Einstein equation exploring the relation between diffusivity and viscosity have a long history, indeed going back to studies of atomic and molecular fluids, where the *approximate* validity of the Stokes–Einstein formula for molecules was well known (Zwanzig and Bixon, 1970).

So, caution must be exercised when the dynamics of the material are interpreted using the GSER. Still, it can be seen as a potential *index* method of rheology, capable of detecting changes due to curing or gelation, for instance. Such methods have been applied to industrial rheology—the curing of paints and coatings, rheological changes that accompany food processing (yogurt, cheese), cements, and similar rheological changes in consumer-care products (Alexander and Dalgleish, 2007; Moschakis, 2013).

3.11 General limits of operation

The exact range of measurable moduli and time scales for passive microrheology depends on the technique that is used. In the next chapters, we will introduce the methods of multiple particle tracking (Chapter 4) and light scattering microrheology (Chapter 5). There are best practices and nuances for each experiment, but here it is useful to consider a few general limits that apply to any experimental passive microrheology method.

Passive microrheology relies on tracking the motion of particles with respect to time to calculate the mean-squared displacement. The range of time scales and displacements that are accessible with each experimental method define its operating regime. There is a lower time limit set by the MSD acquisition rate and an upper limit determined by the total acquisition time of the ensemble average mean-squared displacement. For example, using video microscopy for particle tracking, the video acquisition frame rate f sets the minimum time between video frames, $\tau_{\min} = 1/f$, and thus the shortest lag time for the MSD. In light scattering, the minimum lag time may be as short as tens of nanoseconds—short enough that we may need to take into consideration the particle and fluid inertia.[10] A more common lower limit is $\approx 1\ \mu$s.

3.11.1 Minimum compliance

Consider the accuracy of the particle tracking and the minimum displacement of the probe's movement that can be detected. Let ε be the lower resolution of the position such that the measured mean-squared displacement

$$\langle \Delta\hat{r}^2(\tau)\rangle = \langle \Delta\hat{x}^2(\tau)\rangle + \langle \Delta\hat{y}^2(\tau)\rangle + \langle \Delta\hat{z}^2(\tau)\rangle \tag{3.158}$$

is given by the "true" mean-squared displacement with a minimum value $2\varepsilon^2$ in each direction by

$$\langle \Delta\hat{x}^2(\tau)\rangle = \frac{kT}{3\pi a}\mathcal{J}(\tau) + 2\varepsilon^2. \tag{3.159}$$

Then the *minimum compliance* $\mathcal{J}_{\min}(\tau)$ must exceed

$$\mathcal{J}(\tau) > \frac{6\pi a\varepsilon^2}{k_B T}. \tag{3.160}$$

The minimum compliance is independent of the number of dimensions $\mathbb{D}$ of the mean-squared displacement. For light scattering, $\mathbb{D} = 3$,

[10] In light scattering microrheology, the lower time limit $\tau_{\min}$ is determined under most circumstances by the particle displacement resolution, *i.e.*, the time it takes a particle to diffusive a given length, like 1 nm. The exact value is determined by the scattering geometry, probe scattering properties (size, concentration), and other factors.

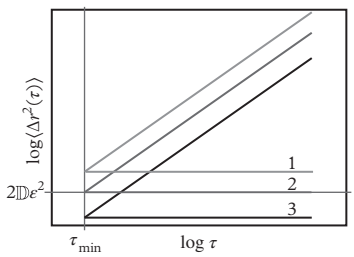

Fig. 3.15 *Limits of the mean-squared displacement.*

while particle tracking is most often performed with a 2D projection of the probe displacement, so $\mathbb{D} = 2$.

We can use eqn 3.160 to identify limits of purely viscous behavior, where $\mathcal{J}(t) = t/\eta$ and purely elastic behavior, where $\mathcal{J}_e = 1/G_e$. Our passive microrheology operating regime is set by the desire to unambiguously distinguish a sample in the two extreme limits of rheological response—a viscous fluid or elastic solid—for $\tau \geq \tau_{\min}$. Figure 3.15 illustrates this heuristic with three sets of MSD curves, corresponding to three Newtonian fluids and three purely elastic solids.

In the first case (1) in Fig. 3.15, both MSD curves for the hypothetical viscous fluid and elastic solid are above $\langle \Delta r^2(\tau) \rangle > 2\mathbb{D}\varepsilon^2$ for $\tau > \tau_{\min}$. Over all lag times, the fluid can be unambiguously distinguished from the elastic solid. Any sample with complex viscoelastic behavior between these limits could also be measured.

In case (2) of Fig. 3.15, the limit is reached wherein the particle motion in the elastic solid cannot be distinguished from the minimum displacement of the method being used. However, any sample in which the creep compliance is above this line will be measurable. When (3) is reached, however, there is a range of lag times for which the displacement in the limiting viscous behavior falls below $2\mathbb{D}\varepsilon^2$. The measured MSD would be constant, then increase after crossing $2\mathbb{D}\varepsilon^2$. Such a cross-over would be smooth and continuous, and thus the short-time or high-frequency response could be mistaken for elasticity even for a sample that is, in reality, purely viscous (Savin and Doyle, 2005).[11] Indeed, comparing eqn 3.118, the resulting curve resembles the expected MSD for a Maxwell fluid.

Maximum viscosity and shear modulus

The general relation eqn 3.160 can be written for the limiting viscosity of a Newtonian fluid,

$$\eta_{\max} = \frac{k_B T \tau_{\min}}{6\pi a \varepsilon^2} \tag{3.161}$$

or the shear modulus amplitude,

$$|G^*(\omega)|_{\max} \approx \frac{k_B T}{6\pi a \varepsilon^2}. \tag{3.162}$$

Using multiple particle tracking microrheology (Chapter 4) and probe particles with diameter $2a = 1\ \mu$m with a typical particle tracking error of $\varepsilon \approx 10$ nm, the calculated limits above are $|G^*(\omega)| \approx 5$ Pa (or $\mathcal{J}_{\min} \approx 0.2\,\text{Pa}^{-1}$) and $\eta_{\max} \approx 150$ mPa · s. But eqn 3.160 also gives the extent to which this range of moduli can be changed by selecting different probe particle sizes. Smaller probes can be used

[11] Savin and Doyle's (2005) data are reproduced in Fig. 4.25.

to increase the upper limits of modulus or viscosity, provided that the continuum approximation of the (generalized) Stokes equation is still satisfied, as Cohen and Weihs (2010) nicely demonstrate in microrheology studies of undiluted, viscous honey samples.

Operating diagram

In Fig. 3.16, we show the operating range of microrheology measurements based on eqns 3.161 and 3.162 in terms of the particle mean-squared displacement and time for three passive microrheology experiments: Multiple particle tracking by video microscopy (MPT), light scattering by diffusing wave spectroscopy (DWS), and single particle laser tracking (LT). Because a common probe particle diameter in microrheology measurements is on the order of 1 μm, we use this probe size to calculate the equivalent values of compliance $\mathcal{J}(t)$, viscosity of a Newtonian fluid η, and equilibrium modulus G_0 of an elastic solid. Again, these limits change with probe size and depend on other experimental factors. For instance, DWS microrheology depends on the scattering geometry and probe concentration. See Chapter 5 for a discussion of these and other details.

Each operating range is bound by a practical upper limit of time scale or lower limit of frequency characterized by the maximum MSD lag time $\tau_{\max}$. If it was certain that the fluid was Newtonian, one could propose to wait an indefinite time for the particles to move a measurable distance. But in practice, it is usually not feasible to track materials over such long times—small amounts of convection could obscure the particles' diffusive motion, or macroscopic vibration and

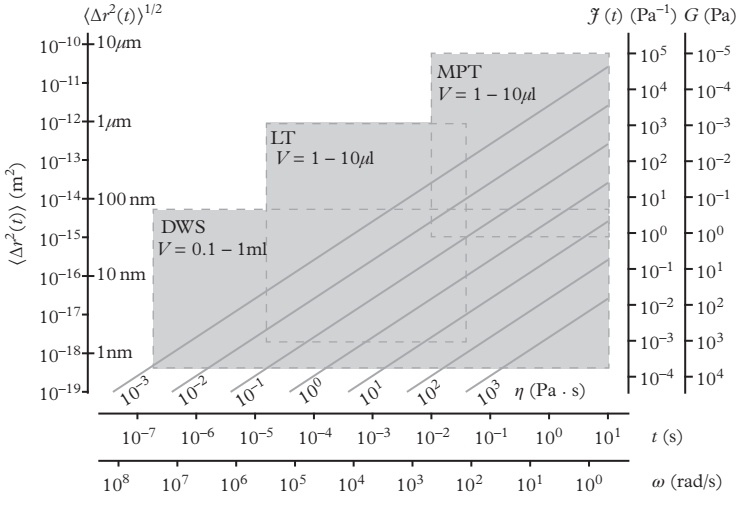

Fig. 3.16 *Operating limits of passive microrheology using multiple particle tracking (MPT), diffusing wave spectroscopy (DWS) and laser tracking (LT). The ranges shown here are calculated for a probe diameter* $2a = 1$ μm. *The limits can be shifted by changing the probe size, provided that this does not violate the continuum assumption of the Stokes equation.*

thermal expansion could contribute to the measured displacement. And there is the overall acquisition time of the measurement to consider; as we discuss later, materials with a rheology that changes with time, during a hydrogelation reaction, for instance, necessitate acquisition times that ensure the ensemble averaged mean-squared displacement approximates a stationary property. One exception is the use of multispeckle imaging discussed in Section 5.7.6.

Typical sample volumes are also indicated in Fig. 3.16. Taken together, the volumes, probe displacements, and time scales identify particular classes of problems amenable to microrheology:

(1) At high compliances, multiple particle tracking is suited to low viscosity samples and the incipient rheology of biomaterial hydrogelators.
(2) At lower compliances and short time scales, diffusing wave spectroscopy can access the terminal relaxation of polymer solutions, networks, and gels. With extended time scales, it can be used to characterize the relaxation time of polymer solutions.
(3) Screening experiments that take advantage of the low volume requirements, and quick mass and heat transfer in samples are.

These and other applications are discussed throughout the text as *application notes* and in Chapter 10.

With the GSER and our understanding of some of the strengths and limitations of passive microrheology, the next two chapters will focus on the experimental methods using microscopy and particle tracking (Chapter 4) and light scattering (Chapter 5).

EXERCISES

(3.1) **Particle in an elastic medium.** Consider the solution to the equation of motion, (eqn 3.1)

$$M_p\dot{\mathbf{V}}(t) = \mathbf{f} - \int_{-\infty}^{t} \zeta(t-t')\mathbf{V}(t')dt', \tag{3.163}$$

in a viscous fluid in the absence of inertia is

$$\mathbf{V} = \mathbf{F}/\zeta, \tag{3.164}$$

where the resistance to motion is represented by a constant memory function (friction coefficient), $\zeta = 6\pi a\eta$. The velocity is a constant that is proportional to ζ. Since ζ is related to the viscosity η, a higher viscosity means that the particle translates more slowly. Show that the solution to the equation of motion for a purely elastic material is

$$\Delta \mathbf{X} = \mathbf{f}/\kappa, \tag{3.165}$$

where $\kappa = 6\pi aG$.

(3.2) **Green-Kubo formulas.** Various *Green-Kubo formulas* relate deterministic transport coefficients to autocorrelation functions of stochastic quantities. One step in the derivation of the GSER,

$$\langle v(0)\tilde{v}(\omega)\rangle = \frac{-\omega^2}{6}\langle \Delta\tilde{r}^2(\omega)\rangle, \tag{3.166}$$

is follows from one such formula.

(a) Show that eq 3.166 is the Fourier-Laplace Transform of the integral

$$D = (1/3)\int_0^\infty \langle \mathbf{v}(0)\cdot\mathbf{v}(t)\rangle dt, \tag{3.167}$$

where $\langle \Delta r^2(t)\rangle = 6Dt$.

(b) Next, derive eqn 3.167 by starting with the formula for displacement

$$\Delta\mathbf{r}(t) = \int_0^t \mathbf{v}(\tau)d\tau \tag{3.168}$$

by noting that the scalar mean-squared displacement is then

$$\langle \Delta r^2(t)\rangle = \int_0^t\int_0^t \langle \mathbf{v}(\tau_1)\cdot\mathbf{v}(\tau_2)\rangle d\tau_1 d\tau_2. \tag{3.169}$$

(3.3) **Fluctuation-dissipation.** A colloidal particle in water is subject to an impulsive force with magnitude f_0. In this problem, we will consider an energy balance on the particle.

(a) As the particle moves after the impulse is applied, how much work W is done on the particle by the surrounding fluid? What is the rate of work $\dot{W}$ done by the fluid?

(b) The rate of work done by the fluid on the particle represents the rate of energy dissipation, $\dot{W}_{\text{out}}$. An energy balance on the particle at equilibrium would yield

$$\dot{W}_{\text{in}} + \dot{W}_{\text{out}} = 0 \tag{3.170}$$

(by convention, work done *on* the particle is negative and work done *by* the particle is positive). The impulsive force gives the particle a kinetic energy $\frac{1}{2}mv^2$. Thus, the rate of work done *on* the particle can be estimated as $\dot{W}_{\text{in}} = \frac{1}{2}mv^2/\tau$, where τ is the time over which the force f_0 acts on the particle (alternatively, $\dot{W}_{\text{in}} = \frac{1}{2}mv^2\delta(t)$, where $\delta(t)$ is the Dirac delta function). At equilibrium, the average kinetic energy should be $\frac{1}{2}kT$ by the equipartition theorem. Show that thermal equilibrium establishes a relationship between the force f_0 and the dissipation of energy via friction. This is (roughly) a statement of the *fluctuation-dissipation theorem*.

(c) Use the velocity autocorrelation and equipartition to show that the magnitude of the Brownian force is given by

$$F = 12\pi a\eta kT. \tag{3.171}$$